

Homonuclear radio frequency-driven recoupling in rotating solids

Andrew E. Bennett,^{a)} Chad M. Rienstra, and Janet M. Griffiths^{b)}

Francis Bitter Magnet Laboratory and Department of Chemistry, Massachusetts Institute of Technology, Cambridge, Massachusetts 02139

Weiguo Zhen^{c)} and Peter T. Lansbury, Jr.^{c)}

Department of Chemistry, Massachusetts Institute of Technology, Cambridge, Massachusetts 02139

Robert G. Griffin

Francis Bitter Magnet Laboratory and Department of Chemistry, Massachusetts Institute of Technology, Cambridge, Massachusetts 02139

(Received 27 February 1998; accepted 4 March 1998)

We discuss several aspects of homonuclear recoupling and longitudinal exchange using rotor-synchronized spin echo sequences in solid state magic-angle spinning (MAS) experiments. These include the accurate measurement of weak dipole–dipole couplings between rare spins, the behavior of dipolar trajectories in multiple spin environments, and chemical shift correlation spectroscopy via polarization exchange. To describe dipolar trajectories accurately, we adopt an approach to the simulation of these experiments which includes finite pulses and the influence of coherence decay. The latter effect becomes competitive with the strength of weak couplings in many experiments, and a simple empirical approach is outlined for the selection of decay parameters. Dipolar trajectories are shown to be dominated by the largest couplings in multiple spin systems via comparison of two and three interacting spins. Two-dimensional correlation spectroscopy based on dipolar exchange among proximate nuclei is illustrated with a uniformly ¹⁵N, ¹³C-labeled sample of the tetrapeptide achatin-II (Gly-L-Phe-L-Ala-L-Asp). In addition, a frequency-selective approach to recoupling dipolar interactions among homonuclear spins is introduced; selective approaches have possible utility in examining weak dipole–dipole couplings in the presence of strong interactions.

© 1998 American Institute of Physics. [S0021-9606(98)00622-9]

I. INTRODUCTION

Dipole–dipole couplings are an important avenue for investigating molecular structure via distance measurements between or among nuclear spins.^{1,2} The magnitudes of relatively large dipole–dipole interactions are sometimes revealed directly in one-dimensional (1D) solid state NMR spectra.³ However, weak dipole–dipole couplings, which contain important information about relatively long internuclear separations, are frequently obscured by larger interactions in the spin Hamiltonian, and in these cases it is necessary to apply special techniques to enhance and observe the weaker interactions selectively. In static samples, various approaches to enhancing dipole–dipole couplings in the presence of other interactions have been developed for both homonuclear⁴ and heteronuclear interactions.^{5–8} Solid state NMR spectra, however, are often acquired with magic-angle spinning (MAS) in order to improve sensitivity and resolution.^{9–11} This method employs mechanical rotation to eliminate dipole–dipole couplings and other second-rank anisotropic interactions. In order to measure the attenuated di-

polar couplings, they must be reintroduced into MAS experiments with rotor-driven^{12–14} or rf-driven recoupling techniques.^{1,2}

The recoupling of heteronuclear interactions in rotating samples is relatively straightforward to achieve with π pulse sequences.^{15,16} The spin Hamiltonian for coupled homonuclear spins, however, is complicated by the noncommutation among the chemical shifts of the nuclei and their dipole–dipole interactions.¹⁷ For weak couplings, the chemical shift interactions dominate, and recoupling (in the absence of radiofrequency irradiation) occurs only at special “rotational resonance” conditions, where the chemical shift difference between two spins matches a multiple of the spinning frequency, $\Delta\delta = m\omega_r$.^{12–14} Rotational resonance provides a means of accurately measuring distances in these cases,^{1,18,19} most conveniently for spins with significant (>50 ppm) chemical shift differences.

Homonuclear recoupling with less sensitivity to the chemical shift is desired for many applications, such as distance measurements between spins of small (<50 ppm) chemical shift differences and correlation spectroscopy of multiple spins over a broad range of chemical shifts.^{20,21} To achieve this goal it is necessary to spoil the coherent averaging of MAS by imposing additional modulations on the spin Hamiltonian with multiple pulse rf irradiation.² The general approach employs applications of rotor-synchronized π and/or $\pi/2$ pulses,^{21–25} continuous (windowless) phase-

^{a)}Present address: Harvard Medical School, 77 Ave. Louis Pasteur, Boston, MA 02115.

^{b)}Present address: Genzyme Corporation, One Kendall Square, Cambridge, MA 02139.

^{c)}Present address: Center for Neurologic Disease, Brigham and Women's Hospital, Harvard Medical School, 77 Ave. Louis Pasteur, Boston, MA 02115.

switched rf fields,^{26–28} or combinations of the two^{29,30} to recouple dipolar interactions. In the more recent experiments,^{26–28,30} recoupling occurs independent of chemical shift terms, albeit with some sensitivity to rf pulse imperfections.

On the other hand, multiple pulse sequences based on π pulses are very robust with respect to rf errors, yet have some remaining dependence on the chemical shift differences among spins. These experiments, monitoring either the transverse²³ or longitudinal evolution^{21,31} of spin magnetization, have been applied to several biophysical applications.^{32–34} Furthermore, as shown here, the rf-driven recoupling (RFDR) approach of π pulse longitudinal exchange is a promising method to measure very long internuclear distances accurately, and it is easily integrated into two-dimensional correlation NMR with multiply ¹³C-labeled samples.^{21,33} In particular, this general approach tolerates pulse errors, and the data is easy to simulate and interpret under typical MAS conditions with the methods described below.

Here we consider the general theory of π pulse recoupling in greater detail using the average Hamiltonian theory (AHT) described by Bennett *et al.*²¹ and also introduce approaches to handling empirically observed signal losses in the interpretation of exchange data. In addition, the two spin and three spin systems are examined to consider the influence of multiple spin couplings in exchange experiments. Under most conditions, the largest dipolar interactions dominate the observed dipolar evolution and obscure the direct impact of weak dipolar couplings.^{18,19,78} Therefore, the observed two-dimensional correlation spectra acquired with this approach and similar nonselective recoupling methods are the result of exchange among spins through their largest dipolar couplings arising from the proximity of nearest neighbors. This phenomenon has been demonstrated with MELODRAMA double-quantum recoupling in multi-spin systems.^{18(b),26} In some cases, it may be desirable to observe the weaker couplings more directly, and a promising approach is to apply frequency-selective recoupling sequences. A method for selective recoupling has already been demonstrated for homonuclear spin systems by application of ramped rf fields¹⁸ and for heteronuclear spins with multi-pulse methods.^{35,36} Here a similar method, based on π pulses, is introduced.

The application of homonuclear recoupling has a promising future in applications to nonoriented biological samples and other systems. The RFDR experiment has already been utilized to examine the retinal-Schiff base linkage³² and Asp-retinal distances in bacteriorhodopsin³⁴ and the analysis of highly ¹³C-enriched chlorophyll/water aggregates using two-dimensional correlation spectroscopy.³³

II. THEORY

A. Average Hamiltonian description of spin echo recoupling

Nuclear spin evolution under rotor-synchronized π pulse sequences can be treated most straightforwardly by the construction of an effective Hamiltonian, which determines the

time evolution operator over multiples of the basic cycle time τ_C . In the case of ideal δ -function π pulses, an effective Hamiltonian can be calculated analytically from either average Hamiltonian theory (AHT)^{37,38} or Floquet theory.^{39,40} Rotor-synchronized rf pulses contribute a time dependence to all spin operators when viewed in the toggling frame.³⁷ In the context of this modulation, the influence of the relatively large chemical shift interactions on the weak dipolar couplings among dilute spins leads to the partial cancellation of their coherent averaging by MAS. In Floquet theory, the recoupling effect is manifest by block diagonalization of the Floquet Hamiltonian with respect to the chemical shift terms, an operation which can be performed analytically.⁴⁰

In the context of AHT, the fact that the chemical shift terms are a cyclic interaction in the rf toggling frame is used to define a second toggling frame, where the AHT approximation is applied only to the remaining part of the internal spin Hamiltonian. The additional terms are the dipolar couplings, which are assumed to be small in the limit $\|H_D\| \tau_C < 1$, $\tau_C = 1/\omega_C$. Under these conditions, the first term of the Magnus expansion provides an adequate expression for the effective dipolar coupling, as well as insight into the mechanism of dipolar recoupling. Since π pulses have no direct effect on the homonuclear dipole-dipole coupling, the reintroduction of the dipolar interaction between two spins results only from the modulation of the spin operators by the difference between their chemical shift interactions and from finite pulse effects.²⁰

In rotational resonance experiments,^{12–14} dipolar recoupling occurs at the special conditions $\Delta\delta = m\omega_r$. When the resonance conditions are satisfied, the relative phase accumulated from the chemical shift interactions cancels after multiples of the rotor cycle. At the same time, the combined time dependence of magic angle spinning and spin operator precession under the chemical shift difference leads to destructive interference and dipolar recoupling. Away from the rotational resonance conditions, the phase arising from the chemical shift evolution fails to cancel over the cycle time and quenches dipolar evolution. It is difficult to define a dominant cyclic interaction away from rotational resonance,⁴⁰ and therefore Floquet theory is particularly useful in determining the nature of the spin dynamics under more general circumstances.^{41–43}

In the case of spin echo sequences under MAS,⁴⁴ the timings of the pulse cycle are constrained by definition to result in the refocusing of the chemical shift interactions, which are eliminated at multiples of the cycle time, τ_C . In rotating solids, the combined time dependence of the amplitude modulation by MAS and the rotations of spin operators by rf pulses must be considered, and rotor synchronization is required in order to guarantee periodicity of the overall time dependence of the system. Figure 1(a) illustrates one class of spin echo sequences for MAS applications, which employs one π pulse per N rotor periods and promotes refocusing of the signal after $2N$ rotor periods.⁴⁴ The basic sequence using $N=1$ has been used to generate dipolar recoupling in transverse SEDRA²³ and longitudinal RFDR^{21,31} experiments.

In order to describe the effect of rotor-synchronized π

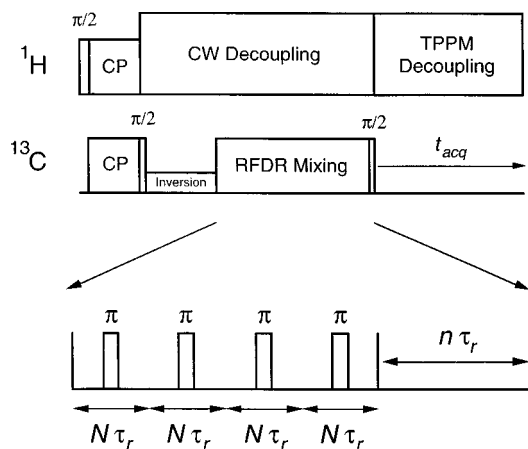


FIG. 1. RFDR pulse sequence for spin echo recoupling, with one π pulse applied per N rotor periods in a one-dimensional inversion exchange experiment. The standard RFDR experiment is performed with $N=1$ and $n=0$. Pulses during mixing are phase cycled according to the XY-16 scheme (Ref. 61). The frequency-selective analog of the mixing sequence employs a non-zero value for n . For two-dimensional chemical shift correlation spectroscopy, an evolution period is inserted (between the ^{13}C CP pulse and $\pi/2$ storage pulse) and the inversion period removed.

pulses on a two spin system, the internal time-dependent Hamiltonian

$$H(t) = \delta_1(t)I_{z1} + \delta_2(t)I_{z2} + d_{12}(t)\{2I_{z1}I_{z2} - I_{x1}I_{x2} - I_{y1}I_{y2}\}, \quad (1)$$

is transformed into a toggling frame defined by the action of the rf pulses. For any $\alpha=x,y,z$ and $\beta=x,y$, an instantaneous π pulse has no effect on the bilinear spin operators

$$\exp\{i\pi(I_{\beta1} + I_{\beta2})\}I_{\alpha1}I_{\alpha2} \exp\{-i\pi(I_{\beta1} + I_{\beta2})\} = I_{\alpha1}I_{\alpha2}, \quad (2)$$

but it flips the sign of the operators I_{z1} and I_{z2}

$$\exp\{i\pi(I_{\beta1} + I_{\beta2})\}I_{zj} \exp\{-i\pi(I_{\beta1} + I_{\beta2})\} = -I_{zj}. \quad (3)$$

Consequently, after the toggling frame transformation of the Hamiltonian, $\tilde{H}(t) = U_{\text{rf}}^{-1}(t,0)H(t)U_{\text{rf}}(t,0)$, where $U_{\text{rf}}(t,0) = T \exp\{-i\int_0^t d\tau H_{\text{rf}}(\tau)\}$, the Hamiltonian can be written in the convenient form

$$\tilde{H}(t) = \delta_1(t)\Phi(t)I_{z1} + \delta_2(t)\Phi(t)I_{z2} + d_{12}(t)\{2I_{z1}I_{z2} - I_{x1}I_{x2} - I_{y1}I_{y2}\}, \quad (4)$$

where the function $\Phi(t)$ is equal to +1 after an even number of π pulses have been applied and -1 following an odd number.

The commutation relations among various terms in the Hamiltonian^{45,46} which were valid before the transformation into the toggling frame continue to hold in the new reference frame. In particular, the Hamiltonian can be written as the sum of two commuting terms $\tilde{H}(t) = \tilde{H}_0(t) + \tilde{H}_1(t)$ in the following way:¹⁴

$$\tilde{H}_0(t) = \frac{1}{2}\{\delta_1(t) + \delta_2(t)\}\Phi(t)[I_{z1} + I_{z2}] + d_{12}(t) \cdot 2I_{z1}I_{z2}; \quad (5)$$

$$\tilde{H}_1(t) = \frac{1}{2}\{\delta_1(t) - \delta_2(t)\}\Phi(t)[I_{z1} - I_{z2}] - d_{12}(t)[I_{x1}I_{x2} + I_{y1}I_{y2}]. \quad (6)$$

With this division of the Hamiltonian, the time evolution of the system over τ_C can be expressed as follows:

$$U(\tau_C,0) = U_{\text{rf}}(\tau_C,0) \exp\left\{-i\int_0^{\tau_C} dt \tilde{H}_0(t)\right\} T \times \exp\left\{-i\int_0^{\tau_C} dt \tilde{H}_1(t)\right\}. \quad (7)$$

Since $\tilde{H}_0(t)$ is self-commuting at all times, as well as independent of the other terms in the spin Hamiltonian, its time evolution is evaluated in the absence of the Dyson time-ordering operator T .

Under modulation by MAS, the term involving $\tilde{H}_0(t)$ straightforwardly cancels after multiples of the rotor period. Likewise, the pulse sequence is chosen to have the cyclic property $U_{\text{rf}}(\tau_C,0) = \pm 1$. The term $\tilde{H}_1(t)$, however, fails to commute with itself at different times and therefore exhibits more complicated spin dynamics.¹⁷

In order to obtain a spin echo following some cycle time $\tau_C = n\tau_r$, the time evolution operator for the chemical shift term of the isolated single spins must vanish

$$T \exp\left\{-i\int_0^{\tau_C} dt \delta_j(t)\Phi(t)I_{zj}\right\} = 1. \quad (8)$$

Because the chemical shift Hamiltonians $\delta_j(t)\Phi(t)I_{zj}$ are self-commuting at different times, the complete refocusing of signals from an uncoupled spin system is obtained under the following condition for the formation of a complete spin echo:

$$\int_0^{\tau_C} dt \delta_j(t)\Phi(t) = 0. \quad (9)$$

When this condition holds, the time evolution operator involving $\tilde{H}_0(t)$ in Eq. (7) is eliminated, and the complete time evolution for the spin system reduces to the form

$$U(\tau_C,0) = T \exp\left\{-i\int_0^{\tau_C} dt \tilde{H}_1(t)\right\}. \quad (10)$$

To address the homogeneous dynamics arising from $\tilde{H}_1(t)$, it is useful to divide the Hamiltonian further into a chemical shift difference term $\tilde{H}_{CS,1}(t)$ and an interaction term $\tilde{H}_{D,1}(t)$

$$\tilde{H}_{CS,1}(t) + \tilde{H}_{D,1}(t) = \frac{1}{2}\{\delta_1(t) - \delta_2(t)\}\Phi(t)[I_{z1} - I_{z2}] - d_{12}(t)[I_{x1}I_{x2} + I_{y1}I_{y2}]. \quad (11)$$

This Hamiltonian can be written more conveniently by using the operators of the 23 subspace for the two spin problem,^{45,46}

$$\begin{aligned} I_x^{23} &= [I_{x1}I_{x2} + I_{y1}I_{y2}], \\ I_y^{23} &= [I_{x1}I_{y2} - I_{y1}I_{x2}], \\ I_z^{23} &= \frac{1}{2}[I_{z1} - I_{z2}]. \end{aligned} \quad (12)$$

These operators obey the usual commutation relations for angular momentum operators, $[I_\alpha, I_\beta] = iI_\gamma$, where (α, β, γ) is a cyclic permutation of (x, y, z) , and their use leads to a concise expression for $\tilde{H}_1(t)$

$$\begin{aligned} \tilde{H}_1(t) &= \tilde{H}_{CS,1}(t) + \tilde{H}_{D,1}(t) \\ &= \{\delta_1(t) - \delta_2(t)\} \Phi(t) I_z^{23} + d_{12}(t) I_x^{23}. \end{aligned} \quad (13)$$

It is also useful to define a phase factor $\chi(t) = \int_0^t d\tau \{\delta_1(\tau) - \delta_2(\tau)\} \Phi(\tau)$, which characterizes the evolution of the chemical shift difference term in the toggling frame. Since the chemical shift terms are not necessarily small compared to the rotor frequency, it is not valid in the most general case to apply AHT directly to Eq. (11). Instead, the time evolution operator is again rearranged as follows:

$$\begin{aligned} U(\tau_C, 0) &= U_{CS,1}(\tau_C, 0) \times T \exp \left\{ -i \int_0^{\tau_C} dt \tilde{H}_{D,1}(t) \right\} \\ &= \exp \{ -i \chi(\tau_C) I_z^{23} \} \times T \exp \left\{ -i \int_0^{\tau_C} dt d_{12}(t) \right. \\ &\quad \left. \times [I_x^{23} \cos \chi(t) + I_y^{23} \sin \chi(t)] \right\}. \end{aligned} \quad (14)$$

A second toggling frame $\tilde{\tilde{H}}_{D,1}(t) = U_{CS,1}^{-1}(t, 0) \tilde{H}_{D,1}(t) U_{CS,1}(t, 0)$ is defined in order to isolate the influence of the chemical shift difference contribution. Under any spin echo sequence (for the moment disregarding error terms) the phase $\chi(\tau_C) = 0$, leaving only the dipolar coupling $\tilde{\tilde{H}}_{D,1}(t)$, which reflects the combined influences of magic angle spinning, rf pulses, and chemical shift interactions.

In order to solve for the homogeneous dynamics of $\tilde{\tilde{H}}_{D,1}(t)$, it is necessary to apply either numerical calculations or an analytical approximation such as the Magnus expansion.^{37,38} In the case of ‘‘dilute’’ spins, such as ^{13}C , ^{15}N , or ^{31}P , the homonuclear dipolar coupling constant between two spins is at most several kHz, so the dipolar couplings are relatively weak compared to typical spinning frequencies. In such cases, the zeroth order average Hamiltonian treatment is sufficient. However, in the case of protons, the AHT approach is applicable only to pairs of well-separated atoms. The chemical shift interaction of each spin j has a time-independent isotropic contribution, as well as an oscillating term arising from the chemical shift anisotropy (CSA)^{17,44}

$$\begin{aligned} \delta_j(t) &= \hat{\delta}_j[m=0] + \sum_{m=-2, m \neq 0}^{m=+2} \hat{\delta}_j[m](\alpha_j, \beta_j) \\ &\quad \times \exp\{im(\omega_r t + \gamma_j)\}; \end{aligned} \quad (15)$$

which depends on the Euler angles $(\alpha_j, \beta_j, \gamma_j)$ of the individual crystallites with respect to the rotor axis frame. The dipolar coupling $d_{12}(t)$, whose orientation is defined by the polar angles (θ, ϕ) of the internuclear vector in the rotor frame,⁴⁴ is fully amplitude modulated and vanishes over multiples of the rotor cycle

$$d_{12}(t) = \sum_{m=-2, m \neq 0}^{m=+2} \hat{d}_{12}[m](\theta) \exp\{im(\omega_r t + \phi)\}, \quad (16a)$$

where

$$d_{ij} = -\frac{\mu_0}{4\pi} \left(\frac{\gamma_i \gamma_j \hbar}{r_{ij}^3} \right), \quad (16b)$$

$$\hat{d}_{ij}[\pm m](\theta_{ij}) = \frac{1}{2} d_{ij} G_{|m|}, \quad (16c)$$

$$G_0 = -\frac{(3 \cos^2 \theta_m - 1)}{2} \frac{(3 \cos^2 \theta_{ij} - 1)}{2}, \quad (16d)$$

$$G_1 = -\frac{3}{4} \sin 2\theta_m \sin 2\theta_{ij}, \quad (16e)$$

$$G_2 = -\frac{3}{4} \sin^2 \theta_m \sin^2 \theta_{ij}. \quad (16f)$$

The AHT result for the generalized echo sequence of one π pulse per N rotor periods is the following, neglecting the CSA:

$$\tilde{\tilde{H}}_{D,1}^{(0)} = -\bar{d}_{12} I_x^{23} = -\frac{1}{2} \bar{d}_{12} [I_{+1} I_{-2} + I_{-1} I_{+2}], \quad (17)$$

where the effective coupling constant (in angular units) has the following form in terms of the isotropic shift difference $\Delta\delta = \hat{\delta}_1[0] - \hat{\delta}_2[0]$:

$$\begin{aligned} \bar{d}_{12} &= \frac{2}{\pi} \sum_{m=1,2} \hat{d}_{12}[m](\theta) \cos(m\phi) \left\{ \frac{\Delta\delta/\omega_r}{m^2 - (\Delta\delta/\omega_r)^2} \right\} \\ &\quad \times (-1)^{m-1} \frac{1}{N} \sin \left\{ \pi N \frac{\Delta\delta}{\omega_r} \right\}. \end{aligned} \quad (18)$$

Using the basic sequence of one π pulse per rotor period where $N=1$, strong recoupling is obtained in the neighborhood of the principal rotational resonance conditions $\Delta\delta = m\omega_r$ with $m=1$ and $m=2$.^{21,23,31}

For all N , at exact rotational resonance, $\Delta\delta = m\omega_r$, and the average Hamiltonian reduces to the form²

$$\tilde{\tilde{H}}_{D,1}^{(0)} = -\hat{d}_{12}[m](\theta) \cos(m\phi) I_x^{23}. \quad (19)$$

In contrast, the analogous Hamiltonian in the absence of π pulses does not depend on the azimuthal angle ϕ about the rotor axis²

$$\tilde{\tilde{H}}_{D,1}^{(0)} = -\hat{d}_{12}[m](\theta) I_x^{23}. \quad (20)$$

From a physical viewpoint, the angle ϕ is expected to appear in the result, since it represents the phase difference between the pulse sequence and the rotationally induced oscillation of the spin interactions. One consequence of this phase dependence is that π pulse recoupling is less efficient than rotational resonance over a powder distribution of crystallites. With increasing N , as illustrated in Fig. 2, the nonvanishing homonuclear coupling is recovered with an increasingly narrow bandwidth in the vicinity of the rotational resonance conditions.

The double toggling frame approach reveals two basic conditions for recoupling by rotor-synchronized sequences consisting only of π pulses: (1) the coherent averaging of all chemical shift interactions and (2) the recovery of a nonzero dipolar coupling from destructive interference between MAS and the motion of the flip-flop operator under the rf-modulated chemical shifts. In order to fulfill the second condition, the term $\exp\{i\chi(t)\}$ must exhibit some nonzero Fourier component at frequencies ω_r or $2\omega_r$. For example, although eight π pulses per rotor period promotes the formation of an

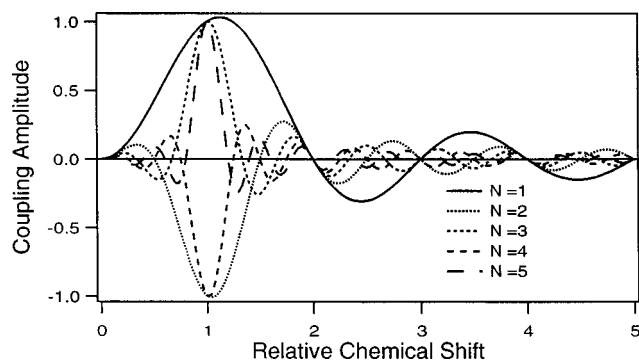


FIG. 2. Relative magnitude of the effective dipole-dipole coupling using various values of N for the $m=1$ Fourier component of the recoupled interaction, according to Eq. (18), as a function of the relative chemical shift difference in units of the spinning frequency, $\Delta\delta/\omega_r$. The $m=2$ Fourier component (not shown) demonstrates similar behavior peaked around the value $\Delta\delta/\omega_r=2$.

echo every rotor period, it does not recouple interactions in the limit of δ -function π pulses.²⁰ In the regime where the spinning speed dominates the CSA, it is reasonable to neglect it in calculating the effective Hamiltonian. With slow spinning, however, the coupling constant becomes a function of the rf-modulated CSA terms, and its influence can be included within the same framework. However, it is more convenient in practice to explore the impact of finite CSA tensors using simulations.

B. Longitudinal exchange and zero-quantum filtering experiments

In the two spin case, as indicated by Eq. (17), a mixing sequence based on π pulses recouples only the flip-flop portion of the dipole-dipole coupling, while the rest of the interaction, $d_{12}(t) \cdot 2I_{z1}I_{z2}$, vanishes exactly over each rotor cycle.¹⁴ Under these conditions, transverse magnetization undergoes dephasing,²³ but not exchange²¹

$$\rho(\tau) = I_{x1} \cos\{\bar{d}_{12}\tau/2\} + 2I_{z1}I_{y2} \sin\{\bar{d}_{12}\tau/2\}. \quad (21)$$

Under δ -function π pulses, or in the absence of rf pulses, exchange of transverse magnetization is forbidden over multiples of the rotor period, since only the flip-flop portion of the spin-spin interaction is recovered. Therefore, in order to use π pulse recoupling in two-dimensional spectroscopy with transverse mixing, $\pi/2$ pulses must be applied for coherence transfer.⁴⁷ On the other hand, the flip-flop coupling directly couples longitudinal polarizations

$$\rho(\tau) = I_{z1} \cos^2\{\bar{d}_{12}\tau/2\} + I_{z2} \sin^2\{\bar{d}_{12}\tau/2\} + [I_{y1}I_{x2} - I_{x1}I_{y2}] \sin\{\bar{d}_{12}\tau\} \quad (22)$$

which implies that longitudinal exchange is the most convenient and straightforward means of acquiring two-dimensional spectra with π pulses. In addition, the spin trajectory develops twice as rapidly in longitudinal exchange compared to the evolution in transverse dephasing, so longitudinal experiments are highly advantageous for the exami-

nation of weak interactions.² In one-dimensional RFDR experiments, the corresponding trajectory begins with a state of inverted relative polarization³¹

$$\rho(\tau) = \frac{1}{2}[I_{z1} - I_{z2}] \cos\{\bar{d}_{12}\tau\} + [I_{y1}I_{x2} - I_{x1}I_{y2}] \sin\{\bar{d}_{12}\tau\}. \quad (23)$$

At any point in the longitudinal trajectory, the zero-quantum (ZQ) coherence [$I_y^{23} = I_{y1}I_{x2} - I_{x1}I_{y2}$] can be eliminated by briefly removing the proton decoupling field, which destroys all spin coherences with transverse character. Although the ZQ coherences are not directly observable, their elimination during the exchange trajectory has a direct impact on the subsequent spin dynamics. In the limit of very rapid decay of zero-quantum coherences, little ZQ coherence is present at all times, and accordingly no change in the dipolar evolution is observed. On the other hand, if its decay rate is negligible, the trajectory of Eq. (23) is modified as follows:

$$\Delta\rho(\tau_1 + \tau_2) = \frac{1}{2}[I_{z1} - I_{z2}] \sin\{\bar{d}_{12}\tau_1\} \sin\{\bar{d}_{12}\tau_2\} + [I_{y1}I_{x2} - I_{x1}I_{y2}] \sin\{\bar{d}_{12}\tau_1\} \cos\{\bar{d}_{12}\tau_2\}, \quad (24)$$

where $\Delta\rho(\tau_1 + \tau_2)$ signifies the difference between the density matrix obtained with and without the removal of the two spin coherences at time τ_1 . This experiment has two applications. First, it provides corroboration that the effective decay parameters for the spin coherences are being selected appropriately for simulations of the experimental data, since these parameters, together with the dipolar coupling constant, reflect how much zero-quantum coherence is present during the trajectory. A second application of this approach is the filtering of signals via the ZQ coherences. Clearly, no signal is obtained from the difference trajectory $\Delta\rho(\tau_1 + \tau_2)$ when the coupling constant d_{12} vanishes, so $\Delta\rho(\tau_1 + \tau_2)$ provides a filtered signal which is maximized when $\tau_1 \approx 1/d_{12}$ and $\tau_1 = \tau_2$.

C. Computational methods for magic-angle spinning and relaxation

In analyzing the evolution of signals under spin echo and other recoupling sequences,^{1,2} analytical approximations provide a basic understanding of the experiments, but for more thorough investigations it is often valuable to perform exact calculations on small sets of coupled spins. In particular, the subtle features of dipolar spin evolution arising from finite pulse effects, higher order contributions to the effective Hamiltonian, and imperfect experimental conditions can be explored with numerical simulations. The essential features of a spin dynamics calculation in the time domain are the construction of the Hamiltonian, the exponentiation of the Hamiltonian to obtain the time evolution operator, and finally the propagation of the density matrix from a given initial condition $\rho(0)$.^{14,48} Other computational approaches to the periodic excitation of spin systems include Floquet theory, which operates essentially in the frequency domain,⁴³ and a mixed approach introduced recently by Levitt and co-workers, where the time and frequency domain approaches are combined.⁴⁹

With a time-dependent Hamiltonian, the time evolution operator $U(\tau,0)$ is divided into short time steps $\Delta\tau$, during which it is a reasonable approximation to regard the Hamiltonian as time independent.⁵⁰ To calculate the macroscopic signal from a polycrystalline solid, the spin trajectories of an isotropic ensemble of crystallite orientations must be calculated in order to compute the integral

$$\langle\langle A(t) \rangle\rangle_{\text{powder}} = \frac{1}{8\pi^2} \int_0^{2\pi} \int_0^\pi \int_0^{2\pi} d\alpha d\beta \times \sin\beta d\gamma \langle A(t; \alpha, \beta, \gamma) \rangle, \quad (25)$$

where $\langle A(t; \alpha, \beta, \gamma) \rangle$ is the expectation value of the signal obtained from a crystallite with Euler angles (α, β, γ) relating the orientation of its molecular axis system to the rotor reference frame. The necessity of calculating the spin trajectory for a large number of crystallite orientations (≥ 100) is the major motivation for optimizing computational efficiency in MAS applications. Numerous recent proposals have addressed the efficiency with which powder averaging may be performed.⁵¹⁻⁵⁴ These methods reduce the number of total crystallites which must be calculated to ensure a given tolerance for precision and systematic error.

In addition, there are several means of efficiently utilizing computer time for calculating the time evolution of individual crystallites. These approaches are frequently applicable and can of course be used in conjunction with the aforementioned powder averaging schemes. First, when the Hamiltonian is periodic, the time evolution operator is required only over one period, and the corresponding evolution of the density matrix can be calculated by applying the same operator repeatedly. This approach is useful in calculating the evolution of nuclear spins under rotor-synchronized recoupling sequences with stroboscopic sampling. A second opportunity arises when the spin Hamiltonian is block diagonal. In many experiments, such as π pulse exchange spectroscopy, periods of free evolution occur between the application of rf pulses. In these cases, the diagonalization of the Hamiltonian matrix is simplified during portions of the spin trajectory. The internal spin Hamiltonian for the two spin system consists of a 4 by 4 matrix with at most a 2 by 2 block in the case of two homonuclear coupled spins,¹⁴ which can be diagonalized analytically.

It is sometimes necessary to include the effects of coherence decay in numerical simulations of spin trajectories. With an exponential model of the decay rates, these calculations require the construction of a supermatrix acting on the set of spin coherences,⁵⁵ greatly increasing the necessary computational effort. The Liouville supermatrix, whose dimensionality spans the square of the number of coherences participating in the trajectory, includes the simultaneous evolution under both the spin Hamiltonian and relaxation effects within an exponential framework. The time-dependent density matrix can be expanded in a convenient orthonormal basis set of Hermitian spin operators as follows:

$$\rho(t) = \sum_m a_m(t) A^m, \quad (26)$$

where orthogonality is defined in the sense: $\text{Tr}\{A^{m*} A^n\} = \delta_{mn}$.⁵⁶ The generalized Liouville equation including exponential relaxation toward equilibrium has the form

$$\frac{d}{dt} \rho(t) = -i[H(t), \rho(t)] - \Gamma\{\rho(t) - \rho_{\text{eq}}\}. \quad (27)$$

With suitable phase cycling, however, it is usually unnecessary to include ρ_{eq} in the analysis of recoupling experiments. Without ρ_{eq} , Eq. (27) can be written more conveniently in terms of the operator expansion

$$\dot{a}_m(t) = \sum_n \{-i \text{Tr}\{A^m[H(t), A^n]\} - \Gamma_{mn}\} a_n(t). \quad (28)$$

With the definition of the matrix elements $L_{mn}(t) = \text{Tr}\{A^m[H(t), A^n]\}$, the Liouville equation can then be formally integrated as follows:

$$a_m(\tau) = \sum_n \left[T \exp \left\{ \int_0^\tau dt (-iL(t) - \Gamma) \right\} \right]_{mn} a_n(0). \quad (29)$$

With the division of the interval $(0, \tau)$ into short time steps $\Delta\tau$ such that $\tau_k = k\Delta\tau$ and $\tau_n = \tau$, the integration of the Liouville operator requires the exponentiations of M by M matrices, where M is the number of coherences participating in the trajectory. For instance, a total of 15 coherences are necessary to span the density matrix for two spins in the most general case.

However, the coherent part of the problem, namely, the exponentiation of the series of matrices $\{-iL(\tau_k)\Delta\tau\}$, requires only the construction of $U(\tau_k, \tau_{k-1})$, which is of much lower dimensionality, e.g., 4 by 4 complex for two spins. In addition, the relaxation process is often taken as time independent and diagonal in a particular basis set of spin coherences.⁵⁷ Consequently, the evolution operator can be divided into its coherent and incoherent components as follows:

$$\begin{aligned} T \exp \left\{ \int_0^\tau dt (-iL(t) - \Gamma) \right\} \\ = \exp\{-iL(\tau_{n-1})\Delta\tau\} \times \exp\{-\Gamma\Delta\tau\} \\ \times \exp\{-iL(\tau_{n-2})\Delta\tau\} \times \exp\{-\Gamma\Delta\tau\} \\ \times \cdots \times \exp\{-iL(\tau_0)\Delta\tau\} \times \exp\{-\Gamma\Delta\tau\}, \end{aligned} \quad (30)$$

which converges in the limit $\Delta\tau \rightarrow 0$. Because the Hamiltonian is time-dependent under MAS and rf pulses, it is already necessary to concatenate the operators obtained with short time steps $\Delta\tau$, and consequently no further computational sacrifice is introduced by applying this approach to relaxation. In fact, the time step required for convergence is generally unchanged with the addition of relaxation effects in practical MAS applications. On the other hand, if the internal Hamiltonian were time-independent as in solution experiments, it would be more computationally efficient to diagonalize the entire M by M matrix just once in order to describe the spin trajectory. The choice of basis operators $\{A^m\}$ can be adjusted to obtain maximum computational efficiency for a given problem. It is generally most natural and

convenient to calculate $\exp\{-iL(\tau_k)\Delta\tau\}$ and $\exp\{-\Gamma\Delta\tau\}$ in different basis sets: the former in the spin eigenstates of z angular momentum and the latter in terms of product operators.⁵⁵ Following the construction of the evolution operators for each time step, they must be transformed into the same basis set. For a time-independent relaxation operator, this operation can be performed once for the relaxation process.

For the recoupling problem discussed here, the spin dynamics calculations used to interpret the dipolar trajectories include empirical estimates of the decay of spin coherences within an exponential model. The observed disappearance of coherences in MAS experiments on highly rigid solids is dominated in many cases by insufficient proton decoupling, which leads to essentially irreversible losses of spin coherences possessing transverse character. A similar analysis of spin trajectories has already been useful in quantitatively understanding the observed dipolar trajectories in heteronuclear recoupling experiments.³⁶

In dipolar trajectories, differential rates of decay among the various coherences perturb the trajectories, particularly when the decay rates are comparable to the magnitude of the dipolar coupling.¹⁴ Kubo and McDowell have introduced approximations of the decay rates of two spin coherences in MAS experiments as the sum of the relevant single spin rates,⁵⁸ a valid approach in the limit where the time-dependent fields causing the disappearance of the signals are independent at each spin. For example, if the spin coherence I_{z1} is taken to disappear exponentially with decay constant Γ_{z1} , and the decay constant of I_{x2} is Γ_{x2} , then the corresponding decay parameter for the two spin coherence $I_{z1}I_{x2}$ is the sum $\{\Gamma_{z1} + \Gamma_{x2}\}$. In the numerical simulations of longitudinal exchange discussed here, this approximation is applied to all of the spin coherences.

D. Influence of finite pulses on spin echo recoupling

In multiple pulse recoupling experiments, the influence of finite pulses is twofold. First, the refocusing of single spin coherences must be robust with respect to errors such as resonance offsets, rf inhomogeneity, and other factors. For example, in the absence of dipole–dipole couplings, the spin echo pulse sequences applied in these experiments must recover all magnetization in the presence of resonance offsets up to approximately $\approx 20\%$ – 40% and rf inhomogeneity of roughly $\pm 5\%$ – 10% of the rf field strength. This compensation is a necessary but not sufficient condition for quantitative results. A second goal of compensated sequences is to generate an effective dipolar coupling which is insensitive to errors in the rf pulses and mechanical rotation.

In the case of π pulse spin echoes, two general approaches to the problem of single spin compensation are the MLEV cycles (i.e., XXXX and its expansions)⁵⁹ and XY-4 (i.e., XYXY with its expansions, XY-8, XY-16, etc.).^{60,61} These cycles are experimentally similar in performance with the exception of situations with significant fixed pulse amplitude imbalances among the phases.⁶¹ However, with digitally controlled quadrature circuits in modern rf transmitters, the amplitude imbalances can routinely be re-

duced to less than 0.1% and phase errors to less than 0.1° .⁶² The MLEV cycles have been applied primarily to windowless proton decoupling in solution NMR spectroscopy. Here we show theoretically that the MLEV and XY cycles are compensated to similar order in the case of long “windows” between the pulses, but that in the windowless case MLEV is generally superior. For this reason, the XY sequences are not likely to compete with the MLEV expansions in continuous-wave applications. However, in the more general case of long inter-pulse windows, their performance is quite similar for single spin recovery with respect to resonance offsets and rf inhomogeneity. In the limit of short windows, the performance of these sequences has been investigated with Floquet theory.⁶³

The treatment discussed here applies to the case of sample spinning under two conditions: The first is that $\tau_r \gg \tau_p$, so that the resonance offset $\delta(t)$ is essentially time-independent during the brief pulse interval τ_p , and the second is that the pulses are applied only at points in time where the offset recurs repeatedly to the same value (i.e., at times separated by multiples of τ_r). The class of echo sequences where the π pulses are applied every N rotor periods possesses this property. These sequences cannot compensate for pulse errors which change from the application of one pulse to the next. Including these effects, the Hamiltonian for a single spin has the form

$$H = H_0 + H_1 = \omega_{\text{rf}} I_x + \{\delta I_z + \Delta\omega_{\text{rf}} I_x\}, \quad (31)$$

during the application of an X pulse, but only $H = \delta S_z$ during the free evolution between the pulses, where δ represents the deviation of the spin frequency from resonance and ω_{rf} is the rf field strength. The $\Delta\omega_{\text{rf}}$ term represents the deviation in the rf field from its nominal value. Although AHT cannot be applied for the entire cycle time τ_C , it is valid for small pulse errors during the pulse time τ_p when $\omega_{\text{rf}} \gg \delta, \Delta\omega_{\text{rf}}$. Through orders $\tilde{H}_D^{(0)}$ and $\tilde{H}_D^{(1)}$, the time evolution operator for the X pulse can be conveniently approximated to $O(\text{error}^2)$

$$\begin{aligned} U_X(\tau_p, 0) &\approx \exp\{-i\omega_{\text{rf}}\tau_p I_x\} \exp\{-i(\tilde{H}_1^{(0)} + \tilde{H}_1^{(1)})\tau_p\} \\ &= \exp\{-i\pi I_x\} \exp\left\{-i\left[\left(\Delta\omega_{\text{rf}} - \frac{1}{2} \frac{\delta^2}{\omega_{\text{rf}}}\right)\tau_p I_x \right. \right. \\ &\quad \left. \left. - \frac{2}{\pi} \left(1 + \frac{\Delta\omega_{\text{rf}}}{\omega_{\text{rf}}}\right)\tau_p I_y\right]\right\}. \end{aligned} \quad (32)$$

In terms of the phase ψ which is accumulated between the pulses, $\psi = \delta(\tau_w - \tau_p)$, and with the convenient definitions

$$a = \frac{4\pi\delta}{\omega_{\text{rf}}} \left\{1 + \frac{\Delta\omega_{\text{rf}}}{\omega_{\text{rf}}}\right\}; \quad b = \pi \left\{-\frac{\delta^2}{2\omega_{\text{rf}}^2} + \frac{\Delta\omega_{\text{rf}}}{\omega_{\text{rf}}}\right\}, \quad (33)$$

the net rotation error through lowest order following the complete XYXY cycle reduces to the form

$$U(\tau_C, 0) = \exp\{+i[(b^2 - a^2)\cos\psi - 2ab\sin\psi]I_z\}. \quad (34)$$

This expression is obtained via the analytical recombination of all consecutive rotations in the pulse cycle with retention of the leading order from the Baker–Campbell–Hausdorff

expansion for recombining small rotations.^{64,65} The condition $U(\tau_C, 0) = \pm 1$ holds for an ideal echo sequence, where no apparent spin evolution occurs over the cycle. Since ψ can assume any value for long windows, the resonance offset effect most generally enters in second order $O(\delta^2/\omega_{rf}^2)$ as a rotation about the z axis, although the performance is compensated to $O(\delta^3/\omega_{rf}^3)$ when $\psi = (2n+1)\pi/2$. In other words, the compensation in $XYXY$ benefits from the phase evolution during the windows. Since the rotation error is oriented along the z axis, the performance of the sequence is worse for transverse magnetization than for recovery of longitudinal magnetization. The analogous expression for $XXX\bar{X}$ (i.e., MLEV-4) is

$$U(\tau_C, 0) = \exp\{+i[(a^2 - b^2)\sin\psi - 2ab\cos\psi]I_z\}. \quad (35)$$

Interestingly, the order of compensation is essentially the same for arbitrary ψ , although the performances of $XYXY$ and $XXX\bar{X}$ differ substantially for particular value of ψ . However, in the windowless limit where $\psi \rightarrow 0$, the $XXX\bar{X}$ cycle is clearly better because the residual error from the offset, for instance, is $O(\delta^3/\omega_{rf}^3)$. A second result of this analysis is that there appears to be no other four pulse cycle with the property of general tolerance to imperfections in pulse rotations.⁶⁰

In order to obtain terms of cubic and higher orders in the rotation error, the AHT treatment of the imperfections during the pulses must be calculated through higher order—or alternatively the error can be derived with exact analytic calculations. The recombination of small rotation operators can likewise be pursued through higher orders. The extension of the basic sequences to eight pulses,⁶¹ $XYXY \rightarrow XYXY YXYX$ and $XXX\bar{X} \rightarrow XXX\bar{X} X\bar{X}X$, cancels the lowest order term along z given by Eqs. (34) and (35), but it leaves a smaller rotation error about an axis within the transverse plane. This deviation is in turn eliminated by expansions to 16 pulse cycles via inversion of all phases.

Although XY cycling does not generally improve the recovery of single spin magnetizations in longitudinal exchange experiments relative to using MLEV, the XY cycles remain highly preferable because of their influence on the form of the effective dipole–dipole coupling. In particular, with the neglect of the chemical shift interactions, the effective dipolar coupling using $XXX\bar{X}$ takes on the following form after averaging over both mechanical rotation and rf pulses in the limit $\tau_p \ll \tau_r$:

$$\begin{aligned} \tilde{H}_{D,1}^{(0)} = & -\frac{3}{4} \left\{ \frac{\tau_p}{\tau_r} \right\} d_{12}(\tau_r/2) [2I_{z1}I_{z2} - I_{x1}I_{x2} - I_{y1}I_{y2}] \\ & -\frac{3}{4} \left\{ \frac{\tau_p}{\tau_r} \right\} d_{12}(\tau_r/2) [I_{x1}I_{x2} - I_{y1}I_{y2}]. \end{aligned} \quad (36)$$

The second term contributes a double quantum operator that is eliminated through zeroth order by the application of an equal number of X and Y π pulses during the full pulse cycle.⁶⁶ For example, using any of the XY sequences or an expansion of MLEV such as $XXX\bar{X} Y\bar{Y}Y$, the pure zero-quantum (i.e., flip–flop) form of the effective Hamiltonian can be maintained with finite pulses, which is a desirable feature in 1D and 2D RFDR experiments. However, since

the expansions of the $XY-4$ sequence in addition provide an excellent means of refocusing single spin errors, they are clearly the best choice for these experiments. For relatively large dipole–dipole couplings and weak π pulses, the first term of Eq. (36) can be fairly significant and leads to significant exchange in strongly coupled spin systems (e.g., in two-dimensional exchange spectroscopy of highly ¹³C-enriched materials).

E. Effect of insufficient proton decoupling

A simple model which is useful in understanding the influence of proton decoupling on the performance of a π pulse consists of the basic Hamiltonian

$$H = \omega_I I_x + \omega_S S_x + d_{IS} \cdot 2I_z S_z, \quad (37)$$

where ω_I and ω_S are the rf field amplitudes applied to the heteronuclear spin pair. The S spin, whose echo intensity is observed, is coupled to the I spin via d_{IS} . With sample rotation, this discussion applies to the case where $\tau_r \gg \tau_p$. Although the decoupling field ω_I is typically applied continuously, the S spin rf field is active only for a short time τ_p in order to stimulate a π pulse rotation. During these intervals, the decoupling efficiency is generally reduced because of interference between the two fields. Moreover, in the case of strong ¹H–¹H interactions, spin coherences involving the protons experience irreversible dephasing within a short time interval,^{56,67} strongly limiting the efficiency of phase-alternated echo sequences in compensating for insufficient proton decoupling. Consequently, it is important to apply strong decoupling on the short time scale τ_p .

The mechanism of decoupling degradation can be understood by examining the time evolution operator during the short interval τ_p when the S spin pulse is applied. The spin operators are transformed into the toggling frame in order to investigate their joint behavior under the two rf fields. To evaluate the time evolution operator, the AHT approximation is employed under the reasonable assumption that both rf fields dominate the dipolar coupling

$$\begin{aligned} U(\tau_p, 0) \approx & \exp\{-i\omega_I\tau_p I_x\} \exp\{-i\omega_S\tau_p S_x\} \\ & \times \exp\{-i\tilde{H}_D^{(0)}\tau_p\}, \end{aligned} \quad (38)$$

where

$$\tilde{H}_D^{(0)} = \frac{1}{\tau_p} \int_0^{\tau_p} dt d_{IS} \cdot 2\tilde{I}_z(t) \tilde{S}_z(t). \quad (39)$$

The evaluation of Eq. (39) leads to the following expression:

$$\begin{aligned}
\tilde{H}_D^{(0)} = & d_{IS} \cdot I_z S_z \left\{ \frac{\sin\{(\omega_I + \omega_S)\tau_p\}}{(\omega_I + \omega_S)\tau_p} + \frac{\sin\{(\omega_I - \omega_S)\tau_p\}}{(\omega_I - \omega_S)\tau_p} \right\} \\
& + d_{IS} \cdot I_z S_y \left\{ \frac{1 - \cos\{(\omega_I + \omega_S)\tau_p\}}{(\omega_I + \omega_S)\tau_p} \right. \\
& \left. - \frac{1 - \cos\{(\omega_I - \omega_S)\tau_p\}}{(\omega_I - \omega_S)\tau_p} \right\} + d_{IS} \\
& \cdot I_y S_z \left\{ \frac{1 - \cos\{(\omega_I + \omega_S)\tau_p\}}{(\omega_I + \omega_S)\tau_p} \right. \\
& \left. + \frac{1 - \cos\{(\omega_I - \omega_S)\tau_p\}}{(\omega_I - \omega_S)\tau_p} \right\} + d_{IS} \\
& \cdot I_y S_y \left\{ \frac{\sin\{(\omega_I + \omega_S)\tau_p\}}{(\omega_I + \omega_S)\tau_p} - \frac{\sin\{(\omega_I - \omega_S)\tau_p\}}{(\omega_I - \omega_S)\tau_p} \right\}.
\end{aligned} \quad (40)$$

Three particular cases deserve attention. First, when the rf fields are matched in amplitude at the Hartmann–Hahn (HH) condition $\omega_S = \omega_I$,⁶⁸ the coherent averaging effect is spoiled by interference between the simultaneous modulations of the I and S spin operators. This resonance condition is fulfilled in cross polarization experiments⁶⁹ in order to permit rotating frame magnetization exchange. In order to minimize dephasing of the signal in spin echo experiments, this HH condition $\omega_S \approx \omega_I$ must clearly be avoided.⁷⁰ However, in the case of a π pulse applied to the S spin, where $\omega_S \tau_p = \pi$, an especially large mismatch is required in order to reduce signal losses to an acceptable level. For example, if $\omega_I = 2\omega_S$, then the dipole–dipole interaction is still not eliminated

$$\tilde{H}_D^{(0)} = -\frac{2}{3\pi} d_{IS} \cdot I_z S_y + \frac{4}{3\pi} d_{IS} \cdot I_y S_z. \quad (41)$$

In order to eliminate $\tilde{H}_D^{(0)}$ over the course of a π pulse, the condition $\omega_I = 3\omega_S$ must be fulfilled, leading to $\tilde{H}_D^{(0)} = 0$.^{64,71} In contrast, over an entire 2π rotation, $\omega_I = 2\omega_S$ is sufficient to ensure $\tilde{H}_D^{(0)} = 0$. Although sharp resonance effects are not observed in practice because of strong proton–proton interactions and sample spinning, this simple model implies that additional decoupling power is required for the case of π pulses compared to windowless ¹³C rf excitations which switch phase less frequently.^{26,28} Over a single cycle τ_p of the decoupling field such that $\omega_I \tau_p = 2\pi$, the coupling vanishes in the absence of the S spin rf field. Since the efficiency of the decoupling field is therefore reduced roughly according to the expression $\omega_I \rightarrow \omega_I - \omega_S$, it is necessary to apply particularly strong proton rf fields during double resonance echo experiments to minimize the decay of S spin coherences. According to Eq. (40), the signal losses should be reduced continuously as the decoupling field and the ratio ω_I/ω_S are increased in the limit $\omega_I \gg \omega_S$.

As will be demonstrated below, it is possible to achieve this limit under some experimental conditions, in which case the rates of coherence loss are extremely small. However, it is not always possible to achieve vanishingly small relaxation rates, either due insufficient available decoupling power or

the presence of molecular motion. Therefore, the quantitative interpretation of recoupling experiments usually requires incorporation of the time scale of coherence losses into numerical calculations.¹⁴ To account for the attenuation of coherences, the exponential framework for describing coherence decay is employed in the π pulse recoupling simulations. An effective rate of decay Γ_p , which is taken to be the same for the longitudinal and transverse spin magnetizations, is chosen to describe dephasing from heteronuclear couplings and random fluctuations in mechanical rotation and rf power. Likewise, an effective T_2 is also selected to match the observed rates of decay in transverse echo recovery experiments. The exponential model accounts for the observed multiple pulse echo intensities reasonably well in polycrystalline solids, and it provides a route to incorporating these influences explicitly into the analysis of dipolar evolution.

F. Frequency-selective experiments

It is desirable in some cases to perform recoupling experiments with frequency selectivity. Rotational resonance is frequency selective in that recoupling occurs only for chemical shift differences $\Delta\delta$ such that $\Delta\delta = m\omega_r$. The selectivity is useful in reducing coupling to the background spins and in providing reference trajectory data without dipolar evolution. An additional possible application of frequency-selective sequences is the direct examination of smaller couplings in the presence of larger ones in isotope-enriched materials.^{18,19,35,36,78} Furthermore, the basic rotational resonance exchange experiment has some disadvantages. Because of the overlapping sideband manifolds between nuclei at rotational resonance, it is sometimes difficult to invert one spin selectively, and sidebands appear at potential cross peak positions in two-dimensional experiments. Here we introduce a multiple-pulse experiment for frequency selectivity in homonuclear spins which is based on π pulse sequences.

The selective sequence in Fig. 1 includes rotor-synchronized periods of delay between sets of four recoupling pulses. For delays of length $n\tau_r$, the average Hamiltonian of Eq. (17) is modified as follows:

$$\tilde{H}_{D,1}^{(0)} = \frac{n}{4+n} \left\{ \Delta\delta - \frac{m}{n} \omega_r \right\} I_z^{23} - \frac{4}{4+n} \bar{d}_{12} I_x^{23}. \quad (42)$$

For weak dipole–dipole couplings, efficient recoupling and dipolar exchange occur only at modified pseudorotational resonance conditions $\Delta\delta = (m/n)\omega_r$. For cases where m/n is not an integer, frequency selectivity occurs away from the conventional rotational resonance conditions. The approach of adding delays between units of pulse cycles is a fairly general means of introducing frequency-selectivity into multiple pulse MAS experiments.

III. EXPERIMENTAL RESULTS AND DISCUSSION

A. Approach to measuring weak dipole–dipole couplings

A primary experimental consideration in attempting to measure weak dipole–dipole couplings with RFDR is the minimization of signal loss due to insufficient ¹H decou-

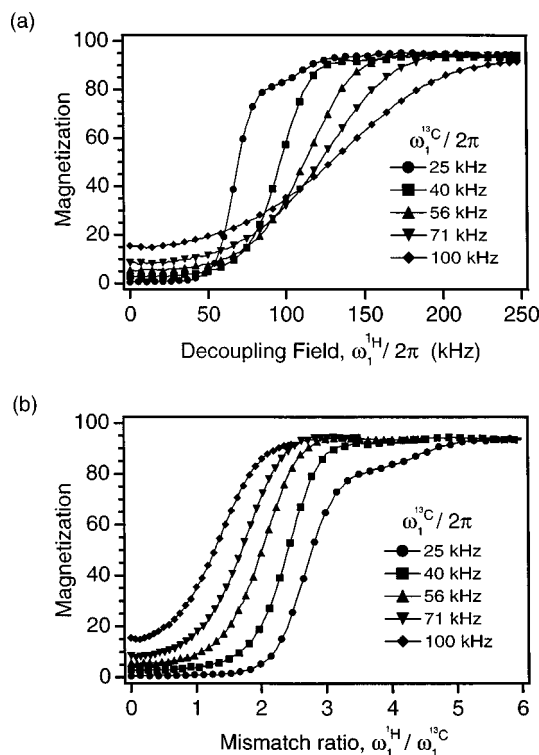


FIG. 3. Experimental determination of magnetization loss under longitudinal mixing. Total ^{13}C magnetization is monitored as a function of ^{13}C rf field (for the π pulses) and ^1H decoupling field (during the π pulses). The ^1H decoupling field between pulses is 150 kHz. Mixing time is 12.8 ms ($64\tau_r$ at 5.000 kHz MAS) with one π pulse per rotor period. Curves are normalized to the signal obtained without a mixing period (CP and $\pi/2$ pulses alone). (a) Plotted as a function of ^1H rf amplitude. (b) Same data as (a), but plotted as a function of the ^1H to ^{13}C rf amplitude ratio. When $\omega_1^{\text{H}}/\omega_1^{13\text{C}} \geq 3$, then minimal ^{13}C magnetization is lost due to depolarization to ^1H (see discussion in the text).

pling. Although effective relaxation rates can easily be measured and included in numerical simulations (*vide infra*), rapid signal loss obscures weak coupling information and reduces the precision with which distance measurements can be performed. The experiments presented in Fig. 3 illustrate that signal losses due to insufficient decoupling can be almost entirely eliminated by appropriate mismatch of the rf field amplitudes. Here we examine the $^{13}\text{CH}_2$ signal of $[2\text{-}^{13}\text{C},^{15}\text{N}]\text{glycine}$, which serves as an excellent test case for decoupling because both the heteronuclear and homonuclear couplings are large (~ 20 kHz).^{72,73}

This sample is particularly difficult to decouple, but separate experiments indicate that under otherwise identical conditions, the directly observed ^{13}C linewidth converges to a constant value (with the lower bound determined by B_0 inhomogeneity and other inhomogeneous broadening) as the on-resonance cw ^1H decoupling field is raised to $\sim 130\text{--}140$ kHz. Furthermore, we do not observe an experimentally significant (~ 0.5 Hz) narrowing observed upon increasing the field from 140 to 250 kHz.⁷⁴ This suggests a complete decoupling of the $^1\text{H}\text{--}^{13}\text{C}$ interactions, which is desirable in the periods between π pulses in order to separate the signal loss due to interference effects alone. Therefore in the experiments here (Fig. 3) we employ a large (150 kHz) ^1H decoupling field between the ^{13}C π pulses. The remaining

loss mechanisms are limited to (1) depolarization due to the interference effect, (2) relaxation through pathways which do not involve the protons (the “true” T_2 in the limit of infinite decoupling, which is greater than 100 ms, as indicated by 95% echo refocusing at 12.8 ms under optimal decoupling conditions), and (3) ^{13}C pulse errors.

The presentation of Fig. 3(b) shows that the 3:1 mismatch is a necessary but not sufficient condition for minimal signal loss. For example, at the lowest ^{13}C field shown here (25 kHz), a steep ascent in echo intensity is observed as the ^1H field is raised to ~ 75 kHz; then the intensity increases at a slower rate until the ^1H field approaches the 130–140 kHz limit. When the 3:1 mismatch already implies a ^1H field of $>130\text{--}140$ kHz, the secondary effect is not significant. Note that although the total signal loss at the higher ^{13}C fields (71 and 100 kHz) with a mismatch of 2–3 is not dramatic, an additional consideration is that the total depolarization contact time is inversely proportional to the ^{13}C field (because the number of π pulses is constant), so the *rate* of polarization decay is well approximated by a function of mismatch alone.

Computationally, the results of Fig. 3 can be described by a coherent three-spin model⁷² in which all spin coherences involving the protons are eliminated between ^{13}C π pulses (simulation data not shown). This is a reasonable physical model because in most organic samples estimates of the correlation time for coherence decay within the proton reservoir ($\tau_c < 30\ \mu\text{s}$) are much shorter than the length of the rotor period (in this case, $\tau_r = 200\ \mu\text{s}$).⁶⁷ The simple three-spin model (without elimination of proton coherences between π pulses) predicts coherent behavior, such as refocusing of $^1\text{H}\text{--}^{13}\text{C}$ antiphase coherences via the XY-16 ^{13}C phase cycling and MAS averaging, which is not observed under the experimental conditions discussed here. Due to the complexity introduced by the large $^{13}\text{C}\text{--}^1\text{H}$ and $^1\text{H}\text{--}^1\text{H}$ couplings, additional resonance effects (where $\omega_1^{\text{H}}/\omega_1^{13\text{C}} = 2n + 1$, $n > 1$) predicted by the zero-order theory of Eq. (40) (and in Ref. 71) do not lead to dramatic behavior in practice. Such effects may be more readily observed at high MAS rates or in samples where the $^1\text{H}\text{--}^1\text{H}$ couplings are weaker.

In experiments where the infinite decoupling limit is not practical, due to the combination of probe limitations and larger ^1H frequency offsets encountered at higher magnetic field, a compromise must be achieved which avoids the steep descent in echo intensity caused by the interference effect. This usually implies raising the ^1H decoupling field during the pulses alone to the maximum level which the probe can safely tolerate, and then strictly obeying the 3:1 mismatch in setting the ^{13}C π pulse. Such an approach was used in the experiments described below, which were performed on probes with limited available ^1H decoupling power.

As we demonstrate in $[2\text{-}^{13}\text{CH}_2,^{15}\text{N}]\text{glycyl}[1\text{-}^{13}\text{COOH}]\text{glycine hydrochloride monohydrate}$, it is still possible to acquire quantitative data under these circumstances. This sample provides a suitable test case for measuring weak homonuclear dipole–dipole couplings with longitudinal π pulse exchange. Its crystal structure is known from neutron diffraction,⁷⁵ and the labeled spin pair has an interatomic separation of 4.56 Å, corresponding to a coupling constant of

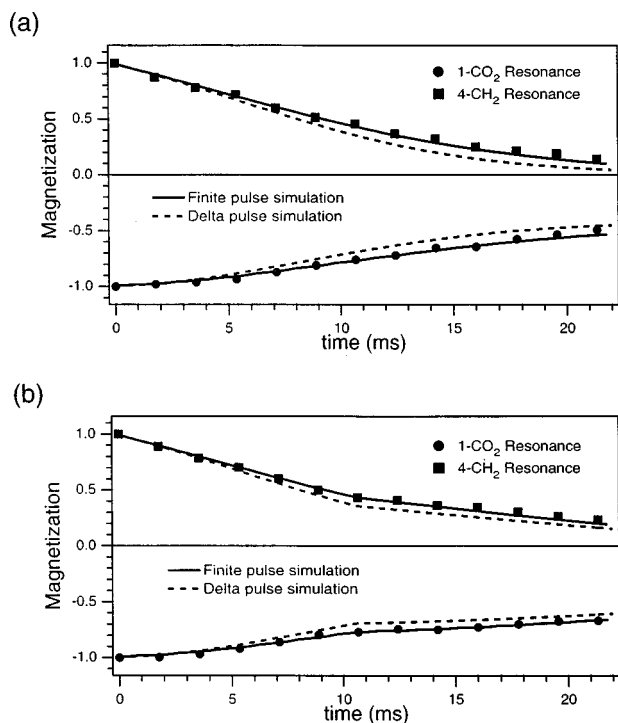


FIG. 4. RFDR inversion exchange results for $[2-^{13}\text{CH}_2, ^{15}\text{N}]$ glycyl- $[1-^{13}\text{COOH}]$ glycine hydrochloride monohydrate (internuclear ^{13}C - ^{13}C distance of 4.56 Å) at 9.00 kHz spinning speed. $^{13}\text{COOH}$ signal intensities are indicated by circles, $^{13}\text{CH}_2$ by squares. The solid lines are corresponding numerical simulations, as described in the text, with finite pulse effects considered; the dotted lines are curves simulated with δ -function pulses. (a) Standard RFDR mixing. (b) RFDR with decoupling turned off at 10.67 ms for two rotor periods, for elimination of zero-quantum coherence.

80 Hz. Figure 4 illustrates longitudinal exchange trajectories for glycyglycine at 9 kHz spinning speed. To interpret the data with numerical simulations, parameters are chosen to match the experimental rates of decay without inversion of the carbonyl spin magnetization. For each nucleus, a single parameter is selected to characterize signal losses arising from each applied π pulse. An effective T_2 is also chosen for each spin based on transverse echo experiments, as demonstrated in Fig. 5. This decay process represents the observed rate of additional decay which occurs during periods of free evolution between the pulses during the echo cycle. The single spin decay parameters are then extended to each coupled spin coherence based on the assumption of uncorrelated fields.⁵⁸ Within this model, the simulations include decay processes for all coherences and the effects of finite pulses.

In the glycyglycine sample, which is 10% diluted in natural abundance material, intermolecular couplings are also expected to influence the experimental exchange trajectories. The crystal structure indicates three significant couplings among separate molecules, with distances 4.26, 4.22, and 4.71 Å, corresponding to dipolar interactions of similar magnitude to that of the intramolecular separation of 4.56 Å. The use of a second moment expansion is helpful in deriving an empirical correction for the intermolecular effects.⁷⁶ The longitudinal exchange trajectory of spin 1 proceeds as follows at times which are short relative to the inverse of the couplings:

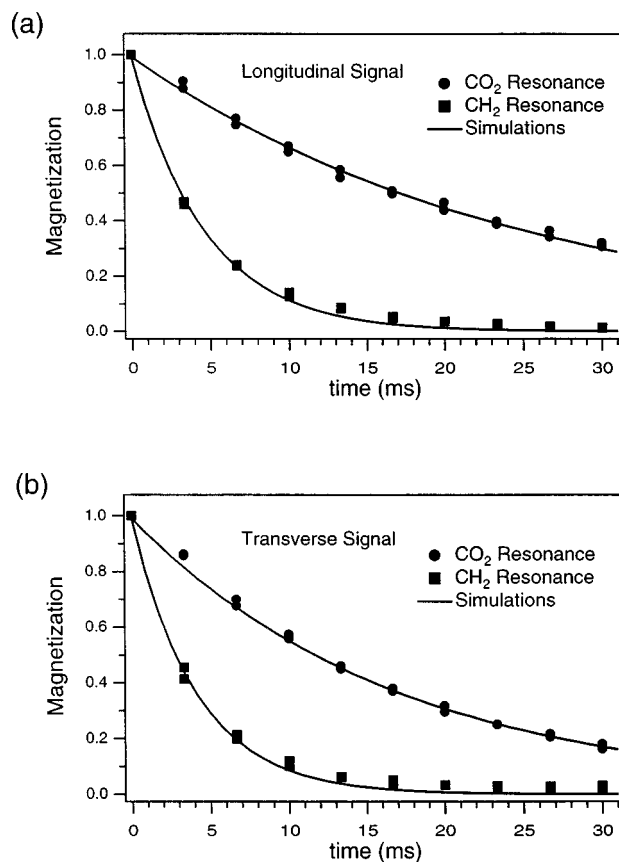


FIG. 5. Echo decay signals of the $^{13}\text{CH}_2$ resonance of glycine where $\omega_1^{\text{H}}/\omega_1^{\text{C}} \approx 3$ (^1H rf field is 70 kHz and ^{13}C rf field is 24 kHz): (a) decay of longitudinal polarization; (b) decay of transverse magnetization. The transverse decay is somewhat more rapid because of insufficient proton decoupling between the pulses and, in principle, slow T_2 relaxation.

$$\langle\langle I_{z1}(\tau) \rangle\rangle \approx 1 - \frac{1}{4} \left\{ \langle \bar{d}_{12}^2 \rangle + \sum_{j \neq 1,2} \langle \bar{d}_{1j}^2 \rangle p_j \right\} \tau^2, \quad (43)$$

where the outer brackets $\langle \dots \rangle$ indicate averaging over the powder distribution. The parameters p_j represent the populations of the intermolecular ^{13}C spins. The following relationship can then be applied to correct the trajectories for the influence of intermolecular interactions

$$x_{12}^{\text{observed}}(\tau) = x_{12}^{\text{actual}}(\tau) + \sum_{j \neq 1,2} x_{1j}^{\text{actual}}(\tau) p_j, \quad (44)$$

where $\langle\langle I_{z1}(\tau) \rangle\rangle = 1 - x_{12}(\tau)$. In the case of the glycyglycine experiment, Eq. (44) implies that the true extent of exchange $x_{12}^{\text{actual}}(\tau)$ is overestimated by about 39% at each point. The experimental points shown in Fig. 4 have been corrected accordingly, leading to good agreement with the simulated finite pulse trajectory with a coupling constant of 85 Hz, which implies an underestimate of 0.1 Å in the internuclear distance. Without the intermolecular correction to the data, the experimental results imply a coupling constant of ≈ 95 Hz, which underestimates the interatomic separation in the molecule by 0.3 Å, a significant error.

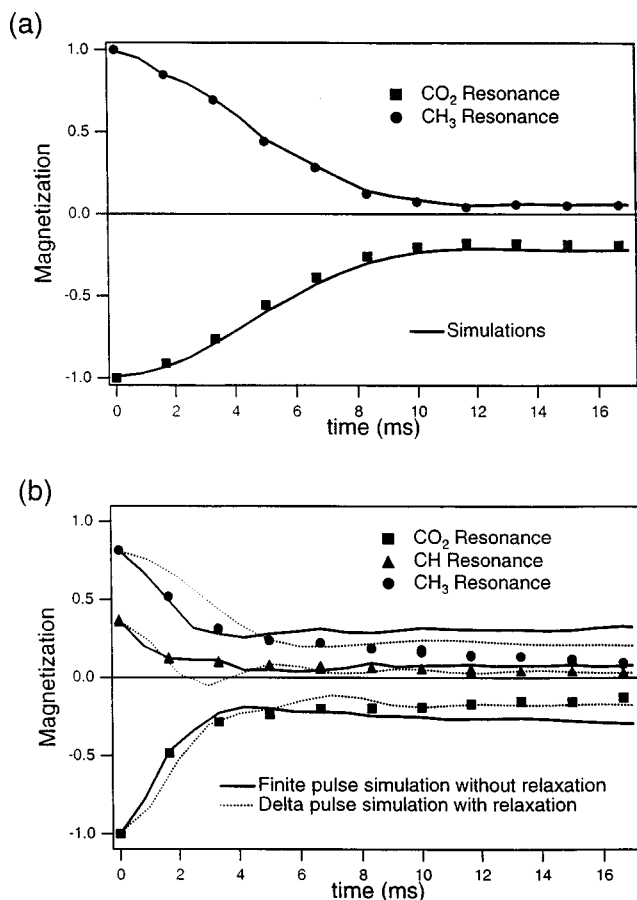


FIG. 6. One-dimensional inversion exchange data at 4.80 kHz spinning speed for (a) [1,3-¹³C,¹⁵N]D,L-alanine and (b) [1,2,3-¹³C]L-alanine, illustrating the influence of the α -¹³C on observed exchange rates using RFDR with one π pulse per rotor period. In both cases, the ¹³COO⁻ resonance was inverted and rotor-synchronized exchange monitored. In case (a), the effects of finite pulses and coherence decay are included in the same simulations. In the three spin case (b), the effects are considered separately for computational convenience.

Figure 4(b) also shows the somewhat modified exchange trajectory which is obtained when the system is perturbed at 10.67 ms by the elimination of the ZQ coherences through the interruption of proton decoupling. The simultaneous agreement of the simulations with the experimental points in both the cases $\tau_1 = 0$ ms and $\tau_1 = 10.67$ ms provides confirmation that the empirical choice of decay parameters describes the nonreversible dephasing of zero-quantum coherences accurately. In the limit of very fast ZQ dephasing, removal of the transverse coherences at 10.67 ms would have no effect on the exchange trajectory. A second application of this approach is the filtering of signals via the ZQ coherences. The difference between the exchanged spectra with and without ZQ interruption at 10.67 ms recovers about 19% of the total signal, which provides a way to obtain the zero-quantum filtered spectrum.

B. Influence of multiple spin interactions

In Fig. 6, the longitudinal exchange trajectories between the carbonyl and methyl nuclei in [1,3-¹³C,¹⁵N]D,L- and [1,2,3-¹³C]L-alanine are compared using the 1D RFDR pulse sequence. In the first case, exchange occurs via the

weak two-spin coupling of 475 Hz.³² In the second trajectory, however, exchange occurs much more rapidly as a result of the additional pathway involving exchange of polarizations via the intervening labeled α -¹³C. In fact, the simulated three-spin trajectories are essentially identical with the deletion of the weaker β -¹³C to CO₂ coupling (not shown for clarity). The exchange process is dominated to a good approximation by the ~ 2 kHz interactions among the directly bonded nuclei,^{18,19,77,78} and proceeds coherently rather than rapidly approaching equilibrium.⁷⁹

The finite pulse simulation for the three spin system with MAS and π pulses is in excellent agreement with the experimental trajectories at short time. However, since the empirical losses of signal are not included, disagreement arises at longer times. A δ -function simulation for the three spin system including signal losses within the same model as above reproduces the decay more accurately at longer times. In both alanine simulations, it is necessary to include explicitly the anomalously short T_1 of 70 ms for the methyl ¹³C of alanine. Since its decay rate is very short compared to those of the other nuclei, the methyl group relaxation directly affects the spin dynamics and cannot be removed by any simple renormalization. In problems involving peptides and proteins in lipids, where dipole-dipole couplings are motionally averaged to some degree and where relaxation is often more rapid than in the rigid samples discussed here, the need to include coherence decay due to molecular motion is likely to arise frequently in practice, and can be considered computationally in the manner discussed here.

C. Frequency-selective homonuclear recoupling

Similar trajectories for [1,3-¹³C,¹⁵N]-alanine using the frequency-selective RFDR approach illustrate that the addition of time delays can quench dipolar evolution away from the resonance conditions. As in similar heteronuclear experiments,^{35,36} selective approaches have potential for the examination of weak couplings in multiple spin environments.^{19,78} In Fig. 7(a), two rotor periods are placed between sets of four rotor periods, during which XY-4 subcycles are completed. For this sequence, recoupling occurs at the experimental spinning frequency of 4.98 kHz, where $\Delta\delta = (5/2)\omega_r$. However, as shown in Fig. 7(b), this evolution is largely quenched when the delay consists of only one rotor period. With a delay of τ_r , recoupling occurs only at the ordinary rotational resonance conditions. At the resonance condition, the small shift between the data and the numerical simulations arises from the finite ¹³C linewidths in the sample (approximately 50 Hz), which contribute small offsets from resonance that slightly quench exchange. This behavior is typical of experiments which depend upon satisfying a sharp resonance condition, such as rotational resonance.^{14,18}

D. Two-dimensional correlation spectroscopy

Two-dimensional (2D) correlation spectra based on the recoupled interactions among neighboring ¹³C spins can be acquired with π pulse longitudinal exchange because Zeeman polarizations are directly coupled via the zero-quantum

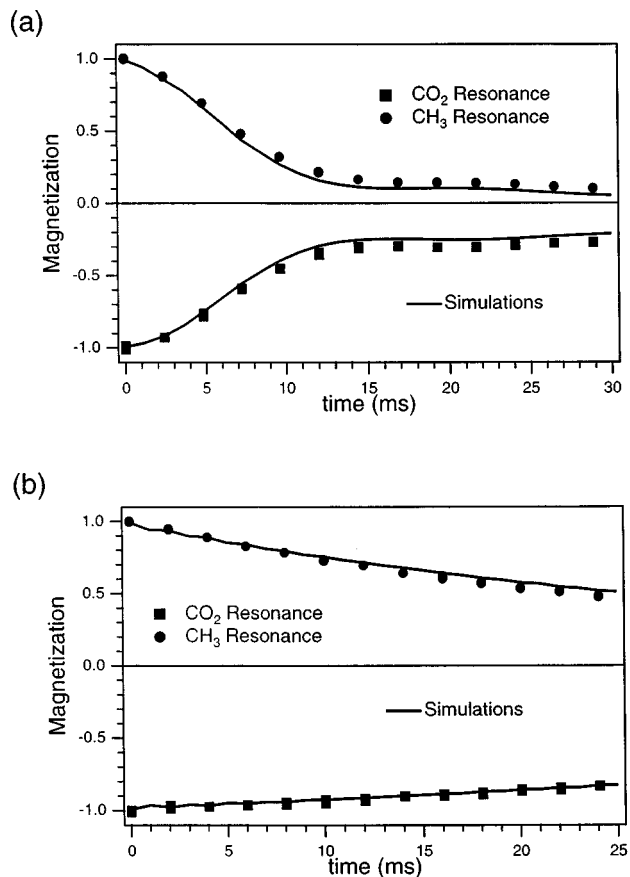


FIG. 7. Frequency-selective RFDR trajectories of $[1,3\text{-}^{13}\text{C},^{15}\text{N}]\text{D,L-alanine}$ employing (a) two rotor periods of delay ($n=2$ in Fig. 1) with exchange at 4.985 kHz spinning speed, where $\Delta\delta=(5/2)\omega_r$, and (b) one rotor period of delay ($n=1$ in Fig. 1), which attenuates dipolar exchange. Finite pulse simulations are indicated by the solid lines.

coherences.²¹ This is illustrated (Fig. 8) in a 2D spectrum of the tetrapeptide achatin-II (Gly-Phe-Ala-Asp).⁸⁰ The relatively short mixing time of 1.55 ms produces crosspeaks between all directly bonded nuclei, including γ_{Phe} to the Phe aromatic ring (not shown). Only correlations within the Phe ring are not evident, due to the degeneracy in shifts and possibly motional effects.

Several interesting features of the spectrum are notable. First, $\omega\text{-}^{13}\text{C}$ to $\alpha\text{-}^{13}\text{C}$ and in one case (Asp) $\beta\text{-}^{13}\text{C}$ to $\gamma\text{-}^{13}\text{C}$, correlations produce the largest crosspeaks (30%–50% of the diagonal), owing to the proximity of these chemical shift differences to the $m=1$ rotational resonance condition. Although RFDR is most efficient in general at recoupling resonances separated approximately by rotational resonance conditions (e.g., $\omega\text{-}^{13}\text{C}$ to $\alpha\text{-}^{13}\text{C}$ at this MAS rate), one- and two-bond exchange also occurs in 1.55 ms between sidechain ^{13}C signals, because of differences in CSA tensor orientations among nearby resonances, as well as the finite pulse recoupling effect described by Eq. (36). The latter effect dominates as the spinning speed increases, which increases the number of pulses applied per unit time. Some sidechain correlations (e.g., $\alpha_{\text{Asp}}\text{-}\beta_{\text{Asp}}$, $\alpha_{\text{Phe}}\text{-}\beta_{\text{Phe}}$) are substantially weaker (10%–20% of diagonal) than the backbone correlations because the chemical shift differences are small; however, they are still easily distinguishable from the inter-

residue ($\omega_i\text{-}\alpha_{i+1}$) crosspeaks which arise at longer mixing times (not shown; a weak $\omega_{\text{Phe}}\text{-}\alpha_{\text{Ala}}$ crosspeak rises just above the lower contour threshold in the spectrum shown). The $\alpha_{\text{Ala}}\text{-}\beta_{\text{Ala}}$ correlation is an intermediate case where the chemical shift difference is a substantial fraction of the MAS rate, and therefore the crosspeak is larger than the other sidechain correlations.

As the Asp motif illustrates, the rate of transfer through directly bonded $^{13}\text{C}\text{-}^{13}\text{C}$ interactions is dominant, with a three-bond intraresidue correlation ($\omega_{\text{Asp}}\text{-}\gamma_{\text{Asp}}$) easily discerned at contour levels where the interresidue three-bond correlations are not. We should emphasize that in no case do direct crosspeaks arise via weaker (<500 Hz) couplings when multistep transfers through intervening larger (500–2.2 kHz) couplings are feasible. Direct measurement of the weaker couplings requires the recoupling effect to be tailored so that the strong couplings are quenched, as in the selective sequence.^{18,19,78}

In cases where uniformity of crosspeak intensities is desired, sequences which are less sensitive to chemical shift differences, such as DRAWS,^{27,81} MELODRAMA,²⁶ and RIL^{30,82} may be used for correlation spectroscopy. However, RFDR presents a very practical means of performing $^{13}\text{C}\text{-}^{13}\text{C}$ correlation spectroscopy because of its robust performance with respect to pulse errors, minimal loss of total polarization, and applicability at very high MAS rates (we have successfully performed such experiments at MAS rates of up to 19 kHz). In addition, the RFDR sequence (in the appropriate MAS regime) is ideally suited for emphasizing backbone $^{13}\text{C}\text{-}^{13}\text{C}$ correlations in peptides and proteins.

IV. EXPERIMENTAL AND NUMERICAL PROCEDURES

A. Experimental details

Experiments were performed with custom-designed NMR spectrometers and probes at several magnetic fields. Features common to all experiments discussed here are the application of XY-16 phase cycling⁶¹ and maintenance of rotor-synchronization within ± 5 Hz with commercial spin rate controllers (Doty Scientific, Columbia, SC) unless indicated otherwise.

The ^1H and ^{13}C field-dependent echo intensity spectra presented in Fig. 3 were acquired at 198.8 MHz ^1H frequency (50.0 MHz ^{13}C). A custom-designed triple resonance transmission line probe with a 5 mm Chemagnetics (Fort Collins, CO) spinner module was used. The transmission line design allows the tuning circuit voltages to be minimized so that maximum decoupling fields are not limited by high-voltage breakdown of circuit components.^{83–85} The maximum decoupling field achievable with this probe for bursts of >25 ms is ~ 300 kHz with ~ 1 kW input power. Experiments presented in Fig. 3 were carried out at 5.000 kHz MAS rate with a total of 64 π pulses (12.8 ms mixing time), and the intensities normalized to that acquired with cross polarization and $\pi/2$ pulses alone.

All one-dimensional (1D) exchange experiments presented here were recorded at 317.4 MHz ^1H frequency (79.9 MHz ^{13}C) using double resonance probes for magic-angle spinning employing commercial spinning assemblies (Doty

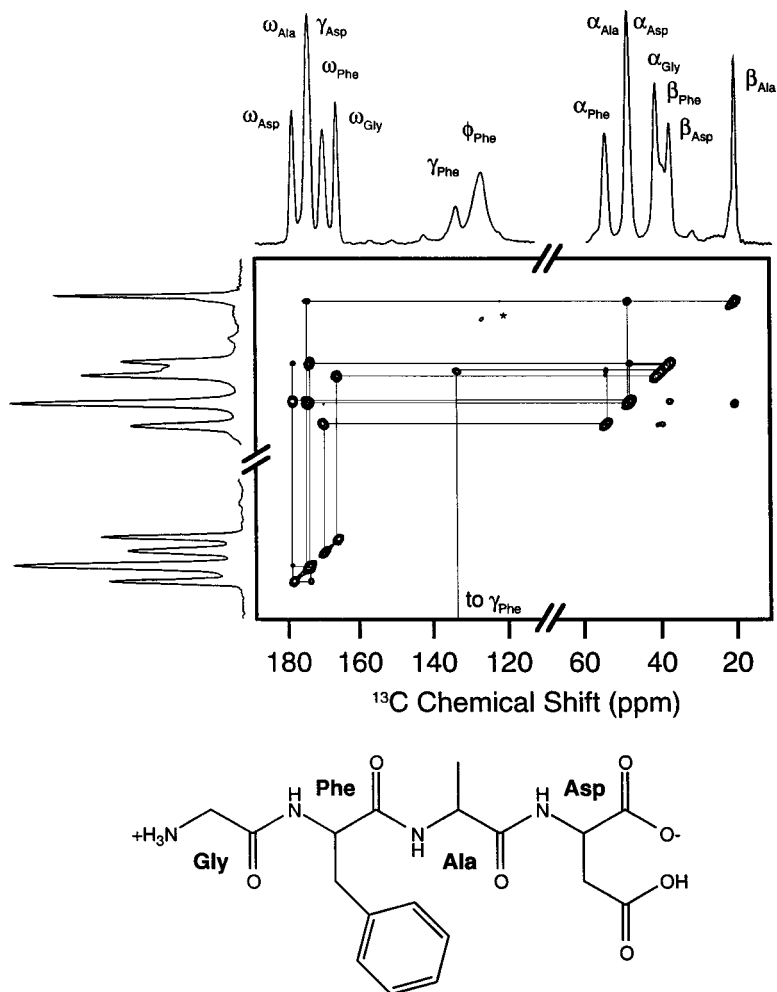


FIG. 8. Two-dimensional ^{13}C - ^{13}C chemical shift correlation spectrum and chemical structure of $[\text{U-}^{13}\text{C}, ^{15}\text{N}]$ achatin-II. RFDR mixing time is 1.55 ms (16 π pulses). Countour levels are logarithmically spaced from 2% to 100% of the maximum peak height. The asterisk indicates a sideband manifold.

Scientific, Columbia, SC). In the 1D exchange trajectories, it is necessary to make corrections to the integrated intensities for the imperfect creation of an inverted state of relative polarization (about 5% error usually), and in addition the contribution from uncoupled background spins must be subtracted from the experimental data.

The 1D experiments in Fig. 4 were performed at 9 kHz spinning frequency using a 5 mm high-speed stator from Doty with π pulse lengths of 15.6 μs for ^{13}C and 5.6 μs for ^1H (89 kHz), corresponding to an amplitude mismatch of 2.8. The chemical shift difference between the 1- $^{13}\text{CO}_2$ and 4- $^{13}\text{CH}_2$ resonances is 10.28 kHz. In the alanine experiments in Fig. 6, the mixing π pulses employed were 20.0 μs , with a ^1H π pulse of 6.2 μs (81 kHz), and the spinning speed was 4.80 kHz. The alanine experiments in Fig. 7 were performed at 4.98 kHz with 18 μs π pulses on ^{13}C . In the single spin glycine echo trajectories (Fig. 5), the spinning speed was 4.80 kHz.

In the two-dimensional RFDR spectrum of achatin, the ^1H frequency is 397.8 MHz (100.0 MHz for ^{13}C); the spinning frequency was 10.309 kHz ± 5 Hz. A triple resonance transmission line probe with 4 mm Chemagnetics spinner module was used. During the mixing period (1.55 ms, 16 π pulses), continuous wave (cw) ^1H decoupling was imple-

mented, with an amplitude of 110 kHz between pulses raised to 150 kHz during the pulses to achieve the appropriate 3:1 mismatch with the 10.0 μs ^{13}C π pulses. TPPM decoupling⁷³ at a reduced field amplitude (80 kHz, 5.8 μs pulse width and total phase difference of 15°) was used during the evolution and acquisition periods. The phase cycling method of Ruben and co-workers was used for pure phase detection in each dimension.⁸⁶

The polycrystalline samples of $[1,3\text{-}^{13}\text{C}, ^{15}\text{N}]$ alanine, $[1\text{-}^{13}\text{C}]$ glycine and $[2\text{-}^{13}\text{C}, ^{15}\text{N}]$ glycine, and $[2\text{-}^{13}\text{CH}_2, ^{15}\text{N}]$ glycyl $[1\text{-}^{13}\text{COOH}]$ glycine hydrochloride monohydrate were diluted tenfold in natural abundance material to reduce the influence of intermolecular dipole-dipole interactions, and recrystallized by slow evaporation from water. Labeled amino acids were purchased from Cambridge Isotope Laboratories (Andover, MA). The tetrapeptide achatin-II (Gly-L-Phe-L-Ala-L-Asp)^{80,87,88} was synthesized via solution methods, which in this case provided far greater coupling efficiency and purity than solid phase methods. Free amino acids were protected with 9-fluorenylmethoxycarbonyl and then converted to their corresponding fluorides,⁸⁹ which were used in the stepwise solution synthesis. This method is efficient with high coupling yield, avoids potential difficulties with racemization, and allows purifica-

tion with one-step preparative HPLC. The lyophilized U-¹³C,¹⁵N-achatin powder was packed in a 4 mm Chemagnetics rotor for NMR experiments.

B. Numerical simulations

In the case of doubly labeled alanine, a decay parameter is chosen to account for the losses of longitudinal spin polarizations during the π pulses, and an effective zero-quantum relaxation time of 32 ms is extracted from the transverse echo trajectories and included in the basic and frequency-selective experiments. Using the known dipolar couplings, the δ -function pulse calculations for the three-spin alanine case include the longitudinal losses within a similar framework and omit the additional transverse decay rates. Because the spinning rates of 4.80 and 4.98 kHz are relatively slow compared to the CSA tensor parameters, these are included in the numerical simulations. For L-alanine, the orientations of the CSA tensors in the crystal reference frame are known from single crystal NMR studies⁹⁰ and explicitly included in the three spin calculations, while the CSA orientations for D,L-alanine are estimated from those of the L-alanine case. The two spin alanine trajectories fit an internuclear distance of 2.51 Å, which is 0.01 Å shorter than obtained from crystallographic studies.⁹¹

For glycylglycine, the anisotropic chemical shifts of the COOH resonance (principal values of -150.9, -36.1, and +6.6 ppm) are included in the calculations. However, for the α -¹³C, only the isotropic shift (68.6 ppm) is included because the CSA is quite small relative to the 9 kHz spinning speed. Although the trajectories are virtually insensitive to the orientation of the CSA in the molecular reference frame, again because of fast MAS, it is included as estimated from the known molecular orientations of carboxyl CSA tensors derived from single crystal studies.⁹² During the pulses, the decay parameters $\Gamma_{\text{COOH}}=24 \text{ s}^{-1}$ and $\Gamma_{\text{CH}_2}=357 \text{ s}^{-1}$ are chosen based on the data acquired without inversion (not shown), while the single spin effective transverse decay rates are $\Gamma_{\text{COOH}}=24 \text{ s}^{-1}$ and $\Gamma_{\text{CH}_2}=8 \text{ s}^{-1}$ during periods of free evolution between the rf pulses. These rates are consistent with minimum observed linewidths, which imply true transverse relaxation rates of $\Gamma \leq 31 \text{ s}^{-1}$ in these rigid systems. With the correction of the experimental points for the overestimate of exchange from intermolecular couplings (as discussed above), the results fit a coupling constant of 85 Hz quite well, as illustrated.

V. CONCLUSIONS

The recoupling of homonuclear interactions using spin echo π pulse sequences and the observation of 1D and 2D exchange is a simple and accurate means of determining internuclear separations and correlations in many cases. Its advantages in measuring weak two-spin couplings include tolerance of the results with respect to rf pulse errors, such as the rf inhomogeneity (up to at least 5% in these experiments) and large CSA tensors, as well as the simplicity of analysis and implementation of experiments and analysis. For weak couplings, the δ -function simulations are reasonably accurate and particularly easy to perform computationally using the

approach to estimating signal losses described here. Compared to rotational resonance, two advantages of this method are that (1) inhomogeneous line broadening does not reduce exchange or complicate its analysis,¹ and (2) spin inversion can be performed straightforwardly away from rotational resonance conditions. Compared to transverse approaches,^{23,47,93} longitudinal evolution is twice as rapid, implying that longer internuclear distances can be examined, and it is more straightforward to apply to two-dimensional correlation spectra. Although spin echo recoupling is most efficient near the $m=1$ and $m=2$ rotational resonance conditions, this range is quite suitable for many ¹³C spectra, which correspond to a similar dispersion at typical magnetic field strengths. In the 2D experiments strong correlations are observed particularly between ω -¹³C and α -¹³C signals. Consequently, π pulse recoupling is a convenient way to obtaining two-dimensional correlation spectra, where spin polarization exchange proceeds via dispersion of magnetizations among neighboring spins.

In cases involving one, two, or three spins, numerical calculations including exponential signal losses are in quantitative agreement with the experimental data. Using this type of analysis, RFDR is applicable to the measurement of distances up to at least 4.56 Å for nuclei with significant chemical shift differences. In the regime of relatively fast spinning, RFDR results also do not depend on the details of the CSA tensors. However, in order to achieve accuracy of 0.1 Å, which is often required in elucidating peptide structure,¹ corrections are necessary for any intermolecular couplings, as well as the inevitable signal decays during the multiple pulse train, and signals from background spins. It should be stressed that observed signal loss rates which differ among the spin coherences do not cancel from the dipolar spin dynamics¹⁴ and must be included in the analysis in cases where the differential decay rates are comparable to the dipole-dipole couplings. Although these problems should be greatly reduced with improved probe technology and decoupling methods,^{73,74} it may be necessary to include coherence decay due to molecular motion in many interesting systems.

As is now well-known^{18,19,26,78} and demonstrated by the three-spin results, exchange with non-selective recoupling sequences proceeds via the strong dipole-dipole couplings in the system. Therefore, in two-dimensional correlation spectra, the migration of spin polarizations occurs via pathways dominated by the nearest neighboring dipole-coupled spins. In this way, a wealth of information concerning the molecular framework of molecules is obtained. However, for applications where the isolation of the weak couplings is particularly desired, the application of frequency-selective π pulse sequences offers an additional approach to selective homonuclear recoupling for cases where rotational resonance conditions^{18,19,78} cannot conveniently be fulfilled. The zero-quantum dephasing experiment also illustrates the potential for efficiently filtering coupled spin signals with couplings ≤ 100 Hz.

ACKNOWLEDGMENTS

The authors wish to acknowledge support of this research by NIH Grants No. RR-00995, GM-36810, GM-

23403, and GM-23289. We also thank Professor Shimon Vega for helpful discussions. Andrew E. Bennett would like to acknowledge predoctoral fellowship support from the National Science Foundation, and Janet M. Griffiths received postdoctoral fellowship support from the American Cancer Society. Chad M. Rienstra is a Howard Hughes Medical Institute Predoctoral Fellow.

- ¹J. M. Griffiths and R. G. Griffin, *Anal. Chim. Acta* **283**, 1081 (1993).
- ²A. E. Bennett, R. G. Griffin, and S. Vega, *NMR Basic Principles and Progress* **33**, 1 (1994).
- ³G. E. Pake, *J. Chem. Phys.* **16**, 327 (1948).
- ⁴H. van Willigen, R. G. Griffin, and R. A. Haberkorn, *J. Chem. Phys.* **67**, 5855 (1977).
- ⁵B. Herzog and E. L. Hahn, *Phys. Rev.* **103**, 148 (1956).
- ⁶M. E. Stoll, A. J. Vega, and R. W. Vaughn, *J. Chem. Phys.* **65**, 4093 (1976).
- ⁷R. K. Hester, J. L. Ackerman, B. L. Neff, and J. S. Waugh, *Chem. Phys. Lett.* **36**, 1081 (1976).
- ⁸R. A. Haberkorn, R. E. Stark, H. van Willigen, and R. G. Griffin, *J. Am. Chem. Soc.* **103**, 2534 (1981).
- ⁹E. R. Andrew, A. Bradbury, and R. G. Eades, *Nature (London)* **182**, 1659 (1958).
- ¹⁰I. J. Lowe, *Phys. Rev. Lett.* **2**, 285 (1959).
- ¹¹J. Schaefer and E. O. Stejskal, *J. Am. Chem. Soc.* **98**, 1030 (1976).
- ¹²B. H. Meier and W. Earl, *J. Am. Chem. Soc.* **109**, 7937 (1987).
- ¹³D. P. Raleigh, M. H. Levitt, and R. G. Griffin, *Chem. Phys. Lett.* **146**, 71 (1988).
- ¹⁴M. H. Levitt, D. P. Raleigh, F. Cruzet, and R. G. Griffin, *J. Chem. Phys.* **92**, 6347 (1990).
- ¹⁵M. G. Munowitz and R. G. Griffin, *J. Chem. Phys.* **76**, 2848 (1982).
- ¹⁶T. Gullion and J. Schaefer, *J. Magn. Reson.* **81**, 196 (1989).
- ¹⁷M. Maricq and J. S. Waugh, *J. Chem. Phys.* **70**, 3300 (1979).
- ¹⁸(a) P. R. Costa, B. Q. Sun, and R. G. Griffin, *J. Am. Chem. Soc.* **119**, 10821 (1997); (b) B.-Q. Sun, C. M. Rienstra, P. R. Costa, J. R. Williamson, and R. G. Griffin, *J. Am. Chem. Soc.* **119**, 8540 (1997).
- ¹⁹P. R. Costa, Ph.D. thesis, Mass. Inst. Tech., 1996.
- ²⁰J. H. Ok, R. G. S. Spencer, A. E. Bennett, and R. G. Griffin, *Chem. Phys. Lett.* **197**, 389 (1992).
- ²¹A. E. Bennett, J. H. Ok, R. G. Griffin, and S. Vega, *J. Chem. Phys.* **96**, 8624 (1992).
- ²²R. Tycko and G. Dabbagh, *Chem. Phys. Lett.* **173**, 461 (1990).
- ²³T. Gullion and S. Vega, *Chem. Phys. Lett.* **194**, 423 (1992).
- ²⁴J. M. Joers, R. Rosanske, T. Gullion, and J. R. Garbow, *J. Magn. Reson., Ser. A* **106**, 123 (1994).
- ²⁵C. A. Klug, W. Zhu, M. E. Merritt, and J. Schaefer, *J. Magn. Reson., Ser. A* **109**, 134 (1994).
- ²⁶B. Q. Sun, P. R. Costa, D. A. Kocisko, P. T. Lansbury, Jr., and R. G. Griffin, *J. Chem. Phys.* **102**, 702 (1995).
- ²⁷D. M. Gregory, D. J. Mitchell, J. A. Stringer, S. Kiihne, J. C. Shiels, J. Callahan, M. A. Mehta, and G. P. Drobny, *Chem. Phys. Lett.* **246**, 654 (1995).
- ²⁸Y. K. Lee, N. D. Kurur, M. Helmle, O. G. Johannessen, N. C. Nielsen, and M. H. Levitt, *Chem. Phys. Lett.* **242**, 304 (1995).
- ²⁹T. Fujiwara, A. Ramamoorthy, K. Nagayama, K. Hioka, and T. Fujito, *Chem. Phys. Lett.* **212**, 84 (1993).
- ³⁰M. Baldus, M. Tomaselli, B. H. Meier, and R. R. Ernst, *Chem. Phys. Lett.* **230**, 329 (1994).
- ³¹D. K. Sodickson, M. H. Levitt, S. Vega, and R. G. Griffin, *J. Chem. Phys.* **98**, 6742 (1993).
- ³²J. M. Griffiths, K. V. Lakshmi, A. E. Bennett, J. Raap, C. M. Vanderwielen, J. Lugtenburg, J. Herzfeld, and R. G. Griffin, *J. Am. Chem. Soc.* **116**, 10178 (1994).
- ³³G. J. Boender, J. Raap, S. Prytulla, H. Oschkinat, and H. J. M. de Groot, *Chem. Phys. Lett.* **237**, 502 (1995).
- ³⁴J. M. Griffiths, A. E. Bennett, J. Herzfeld, and R. G. Griffin (manuscript in preparation).
- ³⁵A. E. Bennett, L. R. Becerra, and R. G. Griffin, *J. Chem. Phys.* **100**, 812 (1994).
- ³⁶A. E. Bennett, C. M. Rienstra, P. T. Lansbury, Jr., and R. G. Griffin, *J. Chem. Phys.* **105**, 10289 (1996).
- ³⁷U. Haeberlen and J. S. Waugh, *Phys. Rev.* **175**, 453 (1968).
- ³⁸U. Haeberlen, *High Resolution NMR in Solids: Selective Averaging* (Academic, New York, 1976).
- ³⁹S. Vega, E. Olejniczak, and R. G. Griffin, *J. Chem. Phys.* **80**, 4832 (1984).
- ⁴⁰A. Schmidt and S. Vega, *J. Chem. Phys.* **96**, 2655 (1992).
- ⁴¹J. M. Shirley, *Phys. Rev. B* **138**, 979 (1965).
- ⁴²D. R. Dion and J. O. Hirschfelder, *Adv. Chem. Phys.* **35**, 265 (1976).
- ⁴³Y. Zur, M. H. Levitt, and S. Vega, *J. Chem. Phys.* **78**, 5293 (1983).
- ⁴⁴E. T. Olejniczak, S. Vega, and R. G. Griffin, *J. Chem. Phys.* **81**, 4804 (1984).
- ⁴⁵A. Wokaun and R. R. Ernst, *J. Chem. Phys.* **67**, 1752 (1977).
- ⁴⁶S. Vega, *J. Chem. Phys.* **68**, 5518 (1978).
- ⁴⁷O. Weintraub, S. Vega, C. Hoelger, and H. H. Limbach, *J. Magn. Reson., Ser. A* **110**, 12 (1994).
- ⁴⁸J. S. Waugh, *J. Magn. Reson.* **50**, 30 (1982).
- ⁴⁹M. Eden, Y. K. Lee, and M. H. Levitt, *J. Magn. Reson., Ser. A* **120**, 56 (1996).
- ⁵⁰F. S. deBouregas and J. S. Waugh, *J. Magn. Reson.* **96**, 280 (1992); S. A. Smith, T. O. Levante, B. H. Meier, and R. R. Ernst, *ibid.* **106**, 75 (1994).
- ⁵¹L. Andreozzi, M. Giordano, and D. Leporini, *J. Magn. Reson., Ser. A* **104**, 166 (1993).
- ⁵²J. M. Koons, E. Hughes, H. M. Cho, and P. D. Ellis, *J. Magn. Reson., Ser. A* **114**, 12 (1995).
- ⁵³D. M. Wang and G. R. Hanson, *J. Magn. Reson., Ser. A* **117**, 1 (1995).
- ⁵⁴M. Bak and N. C. Nielsen, *J. Magn. Reson.* **125**, 132 (1997).
- ⁵⁵R. R. Ernst, G. Bodenhausen, and A. Wokaun, *Principles of Nuclear Magnetic Resonance in One and Two Dimensions* (Clarendon, Oxford, 1987).
- ⁵⁶M. Mehring, *Principles of High Resolution NMR in Solids* (Springer-Verlag, Berlin, 1983).
- ⁵⁷C. P. Slichter, *Principles of Magnetic Resonance* (Springer-Verlag, Berlin, 1990).
- ⁵⁸A. Kubo and C. A. McDowell, *J. Chem. Soc. Faraday Trans.* **84**, 3713 (1988).
- ⁵⁹M. H. Levitt, R. Freeman, and T. Frenkiel, *J. Magn. Reson.* **50**, 157 (1982).
- ⁶⁰A. A. Maudsley, *J. Magn. Reson.* **69**, 488 (1986).
- ⁶¹T. Gullion, D. B. Baker, and M. S. Conradi, *J. Magn. Reson.* **89**, 479 (1990).
- ⁶²D. J. Ruben (private communication).
- ⁶³A. Schmidt and S. Vega, *Isr. J. Chem.* **32**, 215 (1992).
- ⁶⁴A. E. Bennett Ph.D. thesis, Massachusetts Institute of Technology, 1995.
- ⁶⁵Y. Li and J. N. S. Evans, *J. Magn. Reson., Ser. A* **116**, 150 (1995).
- ⁶⁶A. E. Bennett, J. H. Ok, R. G. Griffin, and S. Vega, in *33rd Experimental NMR Conference* (Asilomar, CA, 1992).
- ⁶⁷D. L. VanderHart, W. L. Earl, and A. N. Garroway, *J. Magn. Reson.* **44**, 361 (1981).
- ⁶⁸S. R. Hartmann and E. L. Hahn, *Phys. Rev.* **128**, 2042 (1962).
- ⁶⁹A. Pines, M. G. Gibby, and J. S. Waugh, *J. Chem. Phys.* **59**, 569 (1972).
- ⁷⁰W. P. Aue, D. J. Ruben, and R. G. Griffin, *J. Chem. Phys.* **80**, 1729 (1984).
- ⁷¹Y. Ishii, J. Ashida, and T. Terao, *Chem. Phys. Lett.* **246**, 439 (1995).
- ⁷²U. Haeberlen, *NMR Basic Principles and Progress* **25**, 143 (1990).
- ⁷³A. E. Bennett, C. M. Rienstra, M. Auger, K. V. Lakshmi, and R. G. Griffin, *J. Chem. Phys.* **103**, 6951 (1995).
- ⁷⁴C. M. Rienstra, A. E. Bennett, B. Q. Sun, and R. G. Griffin (manuscript in preparation).
- ⁷⁵T. F. Koetzle, W. C. Hamilton, and R. Parthasarathy, *Acta Cryst., B* **28**, 509 (1972).
- ⁷⁶Y. Pan, T. Gullion, and J. Schaefer, *J. Magn. Reson.* **90**, 330 (1990).
- ⁷⁷(a) M. Munowitz, *Mol. Phys.* **71**, 959 (1990); (b) B. H. Meier, *Adv. Magn. Opt. Reson.* **18**, 1 (1993).
- ⁷⁸P. R. Costa, B.-Q. Sun, and R. G. Griffin (manuscript in preparation).
- ⁷⁹R. Bruschweiler and R. R. Ernst, *J. Magn. Reson.* **124**, 122 (1997).
- ⁸⁰T. Ishida, Y. In, M. Inoue, Y. Yasuda-Kamatani, H. Minakata, T. Iwashita, and K. Nomoto, *FEBS Lett.* **307**, 253–256 (1992).
- ⁸¹D. M. Gregory, M. A. Mehta, J. C. Shiels, and G. P. Drobny, *J. Chem. Phys.* **107**, 28–42 (1997).
- ⁸²M. Baldus and B. H. Meier, *J. Magn. Reson.* **128**, 172 (1997).
- ⁸³R. A. McKay, U.S. Patent #4,446,431 (1984).

- ⁸⁴S. M. Holl, R. A. McKay, T. Gullion, and J. Schaefer, *J. Magn. Reson.* **89**, 620 (1990).
- ⁸⁵R. A. McKay (private communication).
- ⁸⁶D. J. States, R. A. Haberkorn, and D. J. Ruben, *J. Magn. Reson.* **48**, 286 (1982).
- ⁸⁷T. Ishida, Y. In, M. Doi, M. Inoue, Y. Yasuda-Kamatani, H. Minakata, T. Iwashita, and K. Nomoto, *Int. J. Pept. Protein Res.* **39**, 258 (1992).
- ⁸⁸Y. Kamatani, H. Minakata, T. Iwashita, K. Nomoto, Y. In, M. Doi, and T. Ishida, *FEBS Lett.* **276**, 95 (1990).
- ⁸⁹N. C. Chaturvedi, W. D. Fuller, and D. F. Sigler, *Biopolymers* **22**, 2157 (1983).
- ⁹⁰A. Naito, S. Ganapathy, K. Akasaka, and C. A. McDowell, *J. Chem. Phys.* **74**, 3190 (1981).
- ⁹¹M. S. Lehmann, T. F. Koetzle, and W. C. Hamilton, *J. Am. Chem. Soc.* **94**, 2657 (1972).
- ⁹²W. S. Veeman, *Prog. NMR Spectrosc.* **16**, 193 (1984).
- ⁹³O. Weintraub and S. Vega, *J. Magn. Reson.* **105**, 245 (1993).